Repeated Omicron infection alleviates SARS-CoV-2 immune imprinting

Ayijiang Yisimayi[1,2,3,#], Weiliang Song[1,2,3,#], Jing Wang[1,2,3,#], Fanchong Jian[1,2,4,#], Yuanling Yu[2,#], Xiaosu Chen[5], Yanli Xu[6], Sijie Yang[1,7], Xiao Niu[1,3], Tianhe Xiao[1,8], Jing Wang[2], Lijuan Zhao[2], Haiyan Sun[2], Ran An[2], Na Zhang[2], Yao Wang[2], Peng Wang[2], Lingling Yu[2], Qingqing Gu[2], Fei Shao[2], Ronghua Jin[6], Zhongyang Shen[9], Xiaoliang Sunney Xie[1,2], Youchun Wang[2,10], Yunlong Cao[1,2,3*]

[1]Biomedical Pioneering Innovation Center (BIOPIC), Peking University, Beijing, P.R. China.

[2]Changping Laboratory, Beijing, P.R. China.

[3]School of Life Sciences, Peking University, Beijing, P.R. China.

[4]College of Chemistry and Molecular Engineering, Peking University, Beijing, P.R. China.

[5]Institute for Immunology, College of Life Sciences, Nankai University, Tianjin, P. R. China.

[6]Beijing Ditan Hospital, Capital Medical University, Beijing, P.R. China.

[7]Peking-Tsinghua Center for Life Sciences, Tsinghua University, Beijing, P.R. China.

[8]Joint Graduate Program of Peking-Tsinghua-NIBS, Academy for Advanced Interdisciplinary Studies, Peking University, Beijing, P.R. China.

[9]Organ Transplant Center, NHC Key Laboratory for Critical Care Medicine, Tianjin First Central Hospital, Nankai University, Tianjin, P. R. China.

[10]Division of HIV/AIDS and Sex-transmitted Virus Vaccines, Institute for Biological Product Control, National Institutes for Food and Drug Control (NIFDC), Beijing, P.R. China.

[*]Correspondence: Yunlong Cao (yunlongcao@pku.edu.cn).

[#]These authors contributed equally.

Abstract

The continuous emergence of highly immune evasive SARS-CoV-2 variants, like XBB.1.5[1,2] and XBB.1.16[3,4], highlights the need to update COVID-19 vaccine compositions. However, immune imprinting induced by wildtype (WT)-based vaccination would compromise the antibody response to Omicron-based boosters[5-9]. Vaccination strategies that can counter immune imprinting are critically needed. In this study, we investigated the degree and dynamics of immune imprinting in mouse models and human cohorts, especially focusing on the role of repeated Omicron stimulation. Our results show that in mice, the efficacy of single Omicron-boosting is heavily limited by immune imprinting, especially when using variants antigenically distinct from WT, like XBB, while the concerning situation could be largely mitigated by a second Omicron booster. Similarly, in humans, we found that repeated Omicron infections could also alleviate WT-vaccination-induced immune imprinting and generate high neutralizing titers against XBB.1.5 and XBB.1.16 in both plasma and nasal mucosa. By isolating 781 RBD-targeting mAbs from repeated Omicron infection cohorts, we revealed that double Omicron exposure alleviates immune imprinting by generating a large proportion of highly matured and potent Omicron-specific antibodies. Importantly, epitope characterization using deep mutational scanning (DMS) showed that these Omicron-specific antibodies target distinct RBD epitopes compared to WT-induced antibodies, and the bias towards non-neutralizing epitopes observed in single Omicron exposures due to imprinting was largely restored after repeated Omicron stimulation, together leading to a substantial neutralizing epitope shift. Based on the DMS profiles, we identified evolution hotspots of XBB.1.5 RBD and demonstrated the combinations of these mutations could further boost XBB.1.5's immune-evasion capability while maintaining high ACE2 binding affinity. Our findings suggest the WT component should be abandoned when updating COVID-19 vaccine antigen compositions to XBB lineages, and those who haven't been exposed to Omicron yet should receive two updated vaccine boosters.

48 **Main**

49 SARS-CoV-2 continues to evolve, and new mutants constantly emerge under humoral immune
50 pressure[10,11]. New variants, such as the XBB lineages, can evade antibodies induced by vaccination
51 or infection, resulting in repeated infections among populations[5,7,12,13]. Therefore, it is critical to
52 develop updated vaccines that can elicit strong immune responses against the latest variants.

53

54 mRNA vaccine platforms can quickly adapt to new SARS-CoV-2 variants[14-17]. However, since the
55 majority of the population was vaccinated with the ancestral SARS-CoV-2 strain, immune
56 imprinting induced by WT vaccination presents a major challenge to the performance of updated
57 boosters[18,19]. This is because boosting with a variant antigenically distinct from WT would majorly
58 recall memory B cells induced by WT vaccination and masks the *de novo* generation of variant-
59 specific B cells, which would hinder the generation of satisfying humoral immune responses toward
60 new variants[6,7,9,20-23].

61

62 It is crucial to explore vaccination strategies that can counter immune imprinting. In this paper, we
63 investigate the dynamics of immune imprinting in both mouse models and longitudinal human
64 cohorts, with a particular focus on how repeated exposure to Omicron variants could alleviate
65 immune imprinting.

66

67 **Alleviation of immune imprinting in mice**

68 First, we investigated the effects of WT-vaccination-induced SARS-CoV-2 immune imprinting in
69 mice. Two doses of 3 μg CoronaVac (an inactivated vaccine derived from the wildtype SARS-CoV-
70 2) were used as primary immunization and variant Spike proteins were used as boosters[24]. All Spike
71 proteins contained six proline substitutions (S6P) and alanine substitutions in the furin cleavage site
72 to stabilize in prefusion conformation[25].

73 Indeed, mice that received a single booster of 10 μg Spike protein, including BA.1, BA.5, BQ.1.1,
74 XBB, and SARS-CoV-1, had significantly lower serum 50% neutralizing titers (NT50s) (VSV-
75 based pseudovirus) against the boosting variants compared to D614G, revealing substantial immune
76 imprinting at serum level (Fig. 1a and Extended Data Fig.1a). This is consistent with the

77 observations in humans[6,7,20,21,26], as well as previous findings of immune imprinting in influenza
78 viruses[27,28]. Importantly, as the antigenic distance between the boosting variant and the wildtype
79 increased, the overall serum neutralizing activity decreased, and the fold changes between the NT50
80 against the D614G and the boosting variants increased (Fig. 1a and Extended Data Fig. 1b).
81 Importantly, single-dose XBB Spike boosting exhibited the lowest overall neutralizing response. To
82 ensure that the results were not specific to CoronaVac priming, we administered mice with two
83 doses of 10 μg mRNA encoding Spike as primary immunization (Fig. 1b and Extended Data Fig.
84 2a-b). mRNA vaccines also used S6P and alanine substitutions for prefusion-stablization. Similar
85 results were observed when the mRNA vaccines were used as the priming agent, and there were
86 even larger fold changes between NT50s against D614G and the boosting variants (Fig. 1b). To
87 investigate whether prolonging the interval between the primary WT immunization and the variant
88 booster could alleviate immune imprinting, we further tested boosting mice 3-month and 6-month
89 after CoronaVac priming (Fig. 1c). It was observed that 3-month and 6-month intervals between
90 WT-priming and variant-boosting slightly increased overall NT50s, but the fold-change between
91 NT50s against D614G and the boosting variants remained high, especially for XBB (Fig. 1c). This
92 suggests that longer intervals between the priming and Omicron-boosting, which allows the
93 maturation of WT-induced antibodies, may not be sufficient to alleviate immune imprinting.

94 Since the efficacy of the first Omicron booster is heavily limited by immune imprinting, it's crucial
95 to examine how a second Omicron booster performs. We started by boosting CoronaVac-primed
96 mice with two doses of the variant Spike protein over a one-month interval (Fig. 1d). Importantly,
97 the second boosters resulted in greatly increased NT50s against the corresponding variants, as well
98 as substantially reduced fold-changes between the D614G and variants, when compared to the first
99 boosters (Fig. 1d). However, NT50s against the variants still remained lower than those against
100 D614G, and the neutralizing titers against the boosting varirants induced by two Omicron-boosters
101 after priming were even lower than those induced by two doses of variant Spike protein priming,
102 clearly indicating the interference caused by immune imprinting (Extended Data Fig. 3a and Fig.
103 1e). Notably, among the Omicron variants tested, XBB double boosting exhibited the lowest overall
104 titers (Fig. 1d and Extended Data Fig. 3b). Interestingly, these variant boosters, whether protein or
105 mRNA, exhibit different levels of immunogenicity in mice, with XBB demonstrating the lowest

106 (Fig. 1e and Extended Data Fig. 3c).

107 We also tested whether prolonged intervals between Omicron-boosters would facilitate the
108 maturation of variant-specific B cells and enhance the alleviation of immune imprinting (Extended
109 Data Fig.3d). Indeed, a 3-month interval between Omicron boosters resulted in improvements in
110 NT50s against all the corresponding boosting variants, and the fold-change between the NT50s
111 against D614G and the boosting variants substantially decreased, with the XBB boosting group even
112 exhibiting comparable titers to XBB primary (Fig.1d and Extended Data Fig.3a). Interestingly, we
113 observed that prolonging the interval between the first Omicron-booster and the priming series
114 could also improve the performance of the second Omicron-booster (Extended Data Fig. 4a-e).
115 However, the improvement is not as substantial as the ones observed by increasing the time
116 interval between Omicron-boosters, which highlights that the maturation of B cells induced by
117 Omicron-boosting versus those induced by WT-vaccination are more beneficial for immune
118 imprinting mitigation.

119 Since mRNA vaccines encoding Spike have proved to be capable of quick adaptation to new
120 variants, it is critical to test how updated mRNA variant boosters perform, especially when the
121 higher immunogenicity of mRNA vaccine might help alleviate immune imprinting when served
122 as Omicron boosters. Therefore, we tested 1 μg or 10 μg mRNA vaccines encoding BA.5,
123 BQ.1.1, and XBB Spike as boosters in replacement of protein boosters (Extended Data Fig. 5a-
124 d). As expected, 1 μg or 10 μg mRNA vaccine demonstrated higher immunogenicity than the
125 protein vaccine (Fig. 1e). Similarly, the performance of one-dose mRNA Omicron-boosters is
126 still heavily interfered by immune imprinting despite higher immunogenicity, while two mRNA
127 Omicron-boosters would significantly increase antibody titers (Fig. 1f and Extended Data Fig.
128 5a-d). Interestingly, we found that by increasing the dosage of mRNA boosters, repeated mRNA
129 Omicron-boosting can achieve even higher NT50s than 2-dose mRNA priming against the
130 boosting variant, especially demonstrated by XBB mRNA boosting (Extended Data Fig. 5e).
131 This suggests raising the immunogenicity of variant boosters could help to counter immune
132 imprinting brought by WT-vaccination, although this strategy might not be practical in the real
133 world due to safety concerns.

134 Together, our results observed in mice emphasize that the efficacy of the first Omicron booster
135 is severely limited by immune imprinting, especially for those with long antigenic distance
136 from WT, such as XBB, while a second booster is almost mandatory to alleviate immune
137 imprinting and generate high antibody responses.

138

139 **Mitigating immune imprinting in humans**

140 To verify whether the findings from mice also apply to humans, we recruited cohorts with repeated
141 Omicron breakthrough infections (BTIs), including individuals with post-vaccination BA.1 or BA.2
142 BTI followed by BA.5/BF.7 reinfection (BTI+reinfection) and compared them to previously
143 reported BA.1, BA.2, BA.5, BF.7 one-time BTI cohorts[7,26,29]. Importantly, we also included
144 individuals who had no history of SARS-CoV-2 vaccination before repeated infection (vaccination-
145 naïve reinfection) as controls. Detailed information about the cohorts can be found in
146 Supplementary Table 1. We first tested neutralizing titers against exposed variants of these cohorts
147 (Fig. 2a). Similar to mice immunization results, plasma neutralizing titers induced by one-time
148 Omicron BTIs against the corresponding infecting variant were significantly lower than those
149 against D614G, consistent with our previous report[7], and the fold changes between the NT50 against
150 D614G and those against corresponding variants also increased as the antigenic distance increases
151 (Fig. 2a). As expected, in the repeated Omicron infection group, with or without SARS-CoV-2
152 vaccination history, the neutralizing titers against Omicron variants significantly increased
153 compared to one-time BTIs (Fig. 2a-b). More importantly, BA.1 or BA.2 BTI followed by BA.5/
154 BF.7 reinfections demonstrate comparable NT50 between exposed Omicron variants and D614G,
155 indicating immune imprinting alleviation by the second Omicron exposure (Fig. 2a). However, the
156 NT50s of vaccination-naïve reinfection group against Omicron variants were the highest among
157 these cohorts (Fig. 2a), suggesting that repeated BTIs were still subjected to WT-vaccination-
158 induced immune imprinting. Compared to one-time BTIs, repeated Omicron infection also led to an
159 increase in the neutralizing titers against highly immune-evasive CH.1.1, BQ.1.1, XBB, XBB.1.15,
160 XBB.1.16, and XBB.1.5.10 (Fig. 2b and Extended Data Fig. 6a-c), indicating that repeated Omicron
161 infections may broaden the breadth of antibody response. In addition, we found that the nasal swab
162 samples from individuals with repeated Omicron infection exhibited exceptionally high neutralizing
163 titers against Omicron variants, suggesting strong nasal mucosal humoral immunity has been

164 established (Fig. 2c and Extended Data Fig. 6d-f).

165 Neutralization data from both mice and human studies underscore the crucial role of secondary
166 Omicron exposure in mitigating immune imprinting and generating potent antibody responses to
167 immune-evasive variants such as XBB and its sublineages. We propose that this is largely
168 attributable to the further expansion of Omicron-specific memory B cells *de novo* generated by the
169 first Omicron exposure. To assess this hypothesis, we first analyzed the Omicron specificity of
170 RBD-specific memory B cells from BTIs, BTIs+reinfection, and vaccine-naive reinfection cohorts
171 through fluorescence-activated cell sorting (FACS). As we previously reported, in one-time
172 Omicron BTI cohorts, more than 70% of the RBD-binding memory B cells also binded to WT,
173 indicating that post-vaccination Omicron infection mainly recalls cross-reactive memory B cells
174 elicited by WT-based vaccination, but rarely contains BA.1/BA.2-specific B cells (Fig. 3a).
175 Subsequently, following an extended duration of time (8 months) after the first Omicron BTI, the
176 proportion of cross-reactive cells declined while that of Omicron-specific cells increased,
177 suggesting that longer B cell maturation periods elevated the proportion of Omicron-specific
178 memory B cells (Fig. 3b). Nevertheless, at 8 months post-BA.1 BTI, the plasma neutralizing titers
179 were very low due to antibody waning, and thus required a secondary Omicron boosting via either
180 vaccination or infection to increase the antibody levels (Extended Data Fig. 6g). Importantly, for
181 Omicron BTI+reinfection cohorts, the proportion of cross-reactive cells declined further but still
182 remained higher than that observed in the vaccination-naïve reinfection cohort (Fig. 3c-d). These
183 results are highly correlated with the plasma NT50s of the cohorts, which suggests that Omicron-
184 specific antibodies are a major contributor for the increased antibody breadth and neutralization
185 capability after repeated Omicron infection.

186 To further investigate the potency, breadth, and epitopes of these antibodies, the BA.1 RBD-binding
187 cells and BA.2 RBD-binding cells from above various BA.1/BA.2 infection cohorts were sorted and
188 sequenced by high throughput single-cell V(D)J sequencing. Antibodies were then expressed *in*
189 *vitro* as human IgG1 monoclonal antibodies (mAbs) (Supplementary Table 2). For one-time
190 Omicron BTI cohorts, enzyme-linked immunosorbent assay (ELISA) confirmed that only
191 approximately 20% of the isolated mAbs specifically bind to the BA.1/BA.2 RBD and were not
192 cross-reactive to the WT RBD, which was consistent with FACS results (Fig. 3e). Furthermore,

193 long-term sampling (8 months) after BA.1 BTI yielded an increased proportion of BA.1 RBD-
194 specific mAbs compared to short-term (2 months) sampling. Moreover, reinfection with BA.5/BF.7
195 further increased the proportion of BA.1/BA.2 RBD-specific mAbs to around 50%, but this was still
196 lower than that in vaccination-naïve reinfection groups (Fig. 3e). Notably, the somatic
197 hypermutation (SHM) rates of BA.1/BA.2 specific antibodies in BTI+reinfection cohorts were
198 higher than that in one-time BTI cohorts, indicating that BA.1/BA.2 specific antibodies from
199 repeated Omicron infection are more affinity-matured than those without reinfection (Fig. 3f), and
200 the increased affinity maturation of BA.1/BA.2-specific antibodies in response to repeated Omicron
201 infection may contribute to their increased potency against Omicron variants. Together, these data
202 indicate that long-term maturation after one-time Omicron BTI and repeated Omicron infections
203 could significantly raise the proportion and maturation of Omicron-specific antibodies, greatly
204 contributing to the increased plasma neutralization potency against Omicron variants.

205

206 **Epitope analyses of Omicron-specific mAbs**

207 To further interrogate the composition of antibodies elicited by Omicron BA.5/BF.7 BTI and
208 reinfection, and deciphering the molecular mechanism behind the broadly neutralizing capability of
209 convalescent plasma from reinfection, we determined the binding sites and escaping mutations on
210 RBD of these mAbs using deep mutational scanning (DMS)[30,31]. As the proportion of Omicron-
211 specific antibodies is indispensable in reinfection cohorts, and the last exposure of all cohorts
212 involved in this study is BA.5/BF.7, we built a yeast display mutant library based on BA.5 RBD and
213 performed DMS for these mAbs in a high-throughput manner, akin to our previously described WT-
214 based methods[31]. To enhance the sampling of Omicron-specific NAbs to facilitate the epitope
215 characterization of these unprecedented antibodies, we specifically isolated an additional panel of
216 RBD-targeting mAbs that do not cross-bind to WT according to the feature barcode counting during
217 the 10x VDJ sequencing and determined their BA.5-based DMS data. We also determined the BA.5-
218 based DMS data for all BA.5-RBD binding mAbs from previous collections isolated from various
219 immune backgrounds (Supplementary Table 2). In total, a comprehensive panel consisting of 1350
220 mAb BA.5-based DMS is collected.

221

222 By graph-based unsupervised clustering on the determined escape scores over sites on RBD, we
223 identified 12 major epitope groups on BA.5 RBD and embedded the mAbs using UMAP for
224 visualization (Fig. 4a). Names of the epitope groups are generally assigned in line with the epitope
225 groups on WT RBD defined previously[7,26]. Neutralizing activities against SARS-CoV-2 D614G,
226 BA.1, BA.2, BA.5, BA.2.75, BQ.1.1, and XBB.1.5 are determined using VSV-based pseudovirus
227 neutralization assays. In general, neutralization is highly correlated with targeting epitopes of mAbs.
228 Antibodies in epitope groups F3, A1, A2, B, C/D1, D2, D3, D4, and E1/E2.1 target neutralizing
229 epitopes, while antibodies in the other three groups, E2.2, E3, F1, exhibit weak or no neutralization
230 activity (Fig. 4b and Extended Data Fig. 7b). Consistent with the plasma neutralization results, BA.5
231 or BF.7 BTI exhibited substantially imprinted antibody response, leading to over 50% antibodies
232 that target conserved weakly neutralizing epitopes. In contrast, convalescent individuals who
233 experienced BA.5 or BF.7 reinfection after prior BA.1 or BA.2 BTI induce only ~20% antibodies
234 targeting such epitopes, indicating striking alleviation of immune imprinting (Fig. 4c and Extended
235 Data Fig. 7a). Interestingly, prior BA.1 or BA.2 BTI leads to Omicron-specific antibodies targeting
236 distinct epitopes after reinfection. Prior BA.1 BTI induces a higher level of Group D3, while BA.2
237 BTI cohorts consist of more antibodies in Group F3, indicating that the Omicron infection history
238 during repeated Omicron infections would also introduce new Omicron-based immune imprinting.

239

240 Among the 12 identified epitope groups, A1, D2, E1/E2.1, E2.2, E3, and F1 are similar to their
241 corresponding WT-based groups and mainly consist of WT-reactive antibodies (Fig. 4d-e and
242 Extended Data Fig. 7c-d)[26,32]. As expected, BA.5-based epitope landscape also defines novel groups
243 that mainly comprise Omicron-specific mAbs, including Group A2, D3, D4, and F3. Notably, most
244 antibodies in Group F3 here are not cross-reactive to WT RBD as well, which is different from the
245 rare sarbecovirus-neutralizing broad NAbs in Group F3 from SARS convalescents described
246 previously, such as SA55 and BD55-3372[33]. Compared to A1, which mainly contains IGHV3-53/3-
247 66 public antibodies (also known as class 1 or site Ia)[34,35], mAbs in Group A2 are susceptible to
248 mutations on 417 and 505, including the reversions. Group D3 and D4 target an epitope near Group
249 D2 (targeted by LY-CoV1404), but exhibited distinct escape profiles or interacting residues[36]. D3 is
250 susceptible to N439 and K440 mutations, and thus escaped by WT due to N440, while the footprint

251 of D4 is closer to the receptor-binding motif (RBM), interacting with G447, Y449, and R498 (Fig.
252 4d-e). Antibodies in WT-based Group B, C, and D1 have been mostly escaped by L452R, E484A,
253 and F486V in BA.5. B and C/D1 here comprise both WT-reactive and Omicron-specific antibodies,
254 where Group B is more focused on N487 and Y489, and C/D1 mainly focus on F490, which is
255 largely escaped by F490S in XBB variants (Fig. 4d-e and Extended Data Fig. 7c-d). Among the 12
256 groups, A1, A2, B, D3, especially D4 and F3 consist of a substantial proportion of NAbs exhibiting
257 broad neutralization against BQ.1.1 and XBB.1.5 (Fig. 4f). C/D1, D2, and E1/E2.1 also consist of
258 a small proportion of XBB.1.5-neutralizing mAbs (Extended Data Fig. 7f). Considering the recent
259 emergence and prevalence of XBB subvariants harboring F456L (XBB.1.5.10) or K478R
260 (XBB.1.16), which are crucial sites for NAbs in Group A1 and A2, or B and C/D1, respectively, we
261 tested the neutralization of XBB.1.5-neutralizing antibodies from these groups against these two
262 mutants. As expected, F456L escapes or dampens the neutralization of most XBB.1.5-neutralizing
263 antibodies in Group A1 or A2, and XBB.1.16 (E180V+K478R) also escapes a large proportion of
264 NAbs in B and C/D1 (Extended Data Fig. 7e). Overall, these results demonstrate that Omicron
265 repeated infection stimulates a higher level of Omicron-specific neutralizing antibodies targeting
266 neutralizing epitopes compared to one-time Omicron BTI, indicating substantial alleviation of
267 immune imprinted on antibody epitope level. And that these Omicron-specific mAbs have distinct
268 RBD epitopes and escaping mutations compared to WT-induced mAbs would introduce a large
269 neutralizing epitope shift, contributing majorly to the broadly neutralizing capability against
270 XBB.1.5.

271

272 **Evolutionary hotspots on XBB.1.5 RBD**

273 Encouraged by the successful rationalization of the prevalence of F456L and K478R based on DMS,
274 we desire to systematically investigate the evolutionary preference of other RBD mutations. To
275 integratively evaluate the preference of each mutation considering their impacts on neutralizing
276 antibody escape, hACE2 binding, RBD stability, and codon constraints, we previously calculated a
277 weighted preference score for RBD mutations using WT-based DMS profiles and neutralizing
278 activities against BA.5 to predict the convergent evolution of BA.5 RBD[7] (Extended Data Fig. 8).
279 We desire to utilize similar approach with BA.5-based profiles and neutralization against XBB.1.5

280 to identify the evolutionary trends of XBB.1.5 RBD. When considering antibodies from BA.5/BF.7
281 BTI only, the most significant sites include R403S/K, N405K, N417Y, Y453S/C/F, L455W/F/S,
282 F456C/V/L, and Y505H/D, corresponding to escape hotspots of Group A1, A2, and F3 (Fig. 5a).
283 With antibodies from repeated Omicron infection included in the analysis, scores of N439K,
284 K440N/E, K444N/E, and P445S/H/R/L become higher, corresponding to Group D3 and D4, which
285 are consistent with the epitope distributions of mAbs from each cohort (Fig. 5b). Notably, N405D
286 and N417K reversions should hardly appear in the real world due to the potential recovery of
287 previously escaped NAbs in Group F2 and A, respectively. K478 mutations are not identified in the
288 calculation, which is also a limitation of our model due to the low proportion of XBB-neutralizing
289 antibodies in Group B or C/D1 in our cohorts.

290

291 Based on the analysis above, we wonder if the combination of multiple escape mutations against
292 major XBB.1.5-effective epitope groups could essentially evade the broadly neutralizing capability
293 of plasma from repeated Omicron infection while retaining high ACE2 binding affinity. Besides the
294 two emerging mutations K478R and F456L, we selected seven additional substitutions, including
295 H505Y, R403K, K444T, K440N, A484P, Y453F, and N405K, which are sequentially added to
296 XBB.1.5, and constructed seven pseudoviruses named XBB.1.5-S1 to XBB.1.5-S7 (Fig. 6a). The
297 mutations are selected from a larger set of mutation candidates considering their impacts on hACE2-
298 binding affinity as determined by surface plasmon resonance (SPR) and the capability of escaping
299 the neutralization of a panel of 131 potent XBB.1.5-neutralizing antibodies from 8 epitope groups
300 (Fig. 6b-c and Extended Data Fig. 9a). XBB.1.5-S7 successfully escapes the most of NAbs in the
301 panel, except for a small group of broad NAbs from Group F3, A1, and D4, including SA55, a
302 therapeutic antibody under clinical development[33]. Then, we evaluated the neutralization titers of
303 convalescent plasma from individuals who experienced Omicron BTI or repeated Omicron infection
304 against the designed escape mutants. As expected, XBB.1.5-S7 could significantly escape plasma
305 samples from all tested cohorts. Plasma from BA.5 or BF.7 BTI are significantly escaped upon the
306 inclusion of F456L, and nearly negative against XBB.1.5-S7 (Extended Data Fig. 9b). Plasma from
307 repeated Omicron infections is much more resistant to escape mutations. Interestingly, plasma from
308 BA.5/BF.7 reinfection with prior BA.1 BTI or BA.2 BTI exhibited distinct neutralization to different

309 escape mutants. The former samples are largely evaded by K444T and K440N, but not strongly
310 affected by H505Y, while the latter samples are significantly evaded by H505Y (Fig. 6d-e). This is
311 consistent with the observation that reinfection with prior BA.1 BTI elicits more Group D3
312 antibodies, while reinfection with prior BA.2 BTI elicits more Group F3 antibodies (Fig. 4c).
313 Unvaccinated reinfection cohorts exhibited higher neutralization against XBB.1.5 compared to
314 vaccinated cohorts, but equivalently escaped by XBB.1.5-S7. The most significant reduction occurs
315 upon the inclusion of H505Y, K440N, and N405K, indicating a high proportion of Omicron-specific
316 antibodies in Group D3 and F3 (Fig. 6f).

317

318 In summary, our findings suggest that secondary Omicron exposure is necessary to mitigate the
319 immune imprinting conferred by previous ancestral virus exposure and to elicit higher levels of
320 Omicron-specific antibodies. Accordingly, our recommendation is to administer two booster doses
321 of Omicron-based vaccines to individuals who have not received prior Omicron-based vaccinations
322 or who have not been previously infected with the Omicron variant. Moreover, administering the
323 second booster shot after a prolonged interval can provoke a wider and more efficient immune
324 response, while incorporating the wildtype virus into subsequent vaccine designs may worsen
325 immune imprinting[23]. Furthermore, it is imperative to incorporate the XBB variants into vaccine
326 design to achieve broad-spectrum protection, given its potential to mutate and evade vaccines based
327 on previous Omicron variants.

328 Recently, several fast-growing XBB lineages, such as the variant of interest (VOI) XBB.1.16
329 (K478R), XBB.2.3.5 (K478N), and XBB.2.3.4 (K478Q), have acquired RBD mutations on K478.
330 However, the K478 mutation did not emerge in our prediction of evolutionary trends for XBB.1.5
331 RBD. This contradiction may be attributed to the fact that our mutational prediction model primarily
332 relies on the cohorts we recruited, and we haven't captured the immune background that introduced
333 K478 mutation. One possible background that may give rise to K478 is repeated BA.5/BQ.1.1/XBB
334 exposure, as F486 could mask the immunogenicity of K478. Another potential source of K478 is
335 Delta-imprinted convalescents who experienced BA.5/BQ.1.1/XBB infections, which could result
336 in the generation of abundant K478X-sensitive mAbs, given that Delta carries T478K. This may
337 explain why K478X is mostly observed in India[4,37].

338 The degree of immune imprinting might be different between mRNA and inactivated vaccination.
339 Recent studies have shown that subsequently exposed to Omicron twice after two doses of WT-
340 based mRNA vaccines still produce significantly low levels of Omicron-specific antibodies, despite
341 the enhanced neutralization breadth against BQ.1.1 and XBB variants[38,39]. Additionally, individuals
342 who have received two doses of mRNA vaccines and experienced two rounds of Omicron infection
343 also have low levels of Omicron-specific antibodies[38]. This indicates that mRNA vaccines may
344 generate a stronger immune imprinting effect compared to inactivated vaccines, potentially due to
345 its stronger primary humoral immune response[8,40]. However, a head-to-head comparison is needed
346 for validation.

347

348 **References**

349 1 Yue, C. *et al.* ACE2 binding and antibody evasion in enhanced transmissibility of XBB.1.5. *The*
350 *Lancet Infectious Diseases* **23**, 278-280, doi:10.1016/S1473-3099(23)00010-5 (2023).
351 2 Uraki, R. *et al.* Antiviral and bivalent vaccine efficacy against an omicron XBB.1.5 isolate. *The*
352 *Lancet Infectious Diseases* **23**, 402-403, doi:10.1016/S1473-3099(23)00070-1 (2023).
353 3 Yamasoba, D. *et al.* Virological characteristics of the SARS-CoV-2 Omicron XBB.1.16 variant.
354 *bioRxiv*, 2023.2004.2006.535883, doi:10.1101/2023.04.06.535883 (2023).
355 4 Karyakarte, R. P. *et al.* Chasing SARS-CoV-2 XBB.1.16 recombinant lineage in India and the
356 clinical profile of XBB.1.16 cases in Maharashtra, India. *medRxiv*, 2023.2004.2022.23288965,
357 doi:10.1101/2023.04.22.23288965 (2023).
358 5 Kurhade, C. *et al.* Low neutralization of SARS-CoV-2 Omicron BA.2.75.2, BQ.1.1 and XBB.1
359 by parental mRNA vaccine or a BA.5 bivalent booster. *Nat Med* **29**, 344-347,
360 doi:10.1038/s41591-022-02162-x (2023).
361 6 Park, Y. J. *et al.* Imprinted antibody responses against SARS-CoV-2 Omicron sublineages.
362 *Science* **378**, 619-627, doi:10.1126/science.adc9127 (2022).
363 7 Cao, Y. *et al.* Imprinted SARS-CoV-2 humoral immunity induces convergent Omicron RBD
364 evolution. *Nature* **614**, 521-529, doi:10.1038/s41586-022-05644-7 (2023).
365 8 Kaku, C. I. *et al.* Evolution of antibody immunity following Omicron BA.1 breakthrough
366 infection. *bioRxiv*, 2022.2009.2021.508922, doi:10.1101/2022.09.21.508922 (2022).
367 9 Davis-Gardner, M. E. *et al.* Neutralization against BA.2.75.2, BQ.1.1, and XBB from mRNA
368 bivalent booster. *New England Journal of Medicine* **388**, 183-185, doi:10.1056/NEJMc2214293
369 (2022).
370 10 Cox, M. *et al.* SARS-CoV-2 variant evasion of monoclonal antibodies based on in vitro studies.
371 *Nature Reviews Microbiology* **21**, 112-124, doi:10.1038/s41579-022-00809-7 (2023).
372 11 Carabelli, A. M. *et al.* SARS-CoV-2 variant biology: immune escape, transmission and fitness.
373 *Nat Rev Microbiol* **21**, 162-177, doi:10.1038/s41579-022-00841-7 (2023).
374 12 Wang, Q. *et al.* Alarming antibody evasion properties of rising SARS-CoV-2 BQ and XBB
375 subvariants. *Cell* **186**, 279-286 e278, doi:10.1016/j.cell.2022.12.018 (2023).

13 Uraki, R. *et al.* Humoral immune evasion of the omicron subvariants BQ.1.1 and XBB. *Lancet Infect Dis* **23**, 30-32, doi:10.1016/S1473-3099(22)00816-7 (2023).

14 Choi, A. *et al.* Safety and immunogenicity of SARS-CoV-2 variant mRNA vaccine boosters in healthy adults: an interim analysis. *Nature Medicine* **27**, 2025-2031, doi:10.1038/s41591-021-01527-y (2021).

15 Zhang, N.-N. *et al.* Rapid development of an updated mRNA vaccine against the SARS-CoV-2 Omicron variant. *Cell Research* **32**, 401-403, doi:10.1038/s41422-022-00626-w (2022).

16 Scheaffer, S. M. *et al.* Bivalent SARS-CoV-2 mRNA vaccines increase breadth of neutralization and protect against the BA.5 Omicron variant in mice. *Nature Medicine* **29**, 247-257, doi:10.1038/s41591-022-02092-8 (2023).

17 Collier, A.-r. Y. *et al.* Immunogenicity of BA.5 Bivalent mRNA Vaccine Boosters. *New England Journal of Medicine* **388**, 565-567, doi:10.1056/NEJMc2213948 (2023).

18 Aguilar-Bretones, M., Fouchier, R. A. M., Koopmans, M. P. G. & van Nierop, G. P. Impact of antigenic evolution and original antigenic sin on SARS-CoV-2 immunity. *The Journal of Clinical Investigation* **133**, doi:10.1172/JCI162192 (2023).

19 Chemaitelly, H. *et al.* Immune imprinting and protection against repeat reinfection with SARS-CoV-2. *N Engl J Med* **387**, 1716-1718, doi:10.1056/NEJMc2211055 (2022).

20 Kaku, C. I. *et al.* Recall of preexisting cross-reactive B cell memory after Omicron BA.1 breakthrough infection. *Science Immunology* **7**, eabq3511, doi:doi:10.1126/sciimmunol.abq3511 (2022).

21 Quandt, J. *et al.* Omicron BA.1 breakthrough infection drives cross-variant neutralization and memory B cell formation against conserved epitopes. *Science Immunology* **7**, eabq2427, doi:doi:10.1126/sciimmunol.abq2427 (2022).

22 Miller, J. *et al.* Substantial Neutralization Escape by SARS-CoV-2 Omicron Variants BQ.1.1 and XBB.1. *New England Journal of Medicine* **388**, 662-664, doi:10.1056/NEJMc2214314 (2023).

23 Wang, Q. *et al.* SARS-CoV-2 neutralising antibodies after bivalent versus monovalent booster. *The Lancet Infectious Diseases* **23**, 527-528, doi:10.1016/S1473-3099(23)00181-0 (2023).

24 Gao, Q. *et al.* Development of an inactivated vaccine candidate for SARS-CoV-2. *Science* **369**, 77-81, doi:10.1126/science.abc1932 (2020).

25 Hsieh, C.-L. *et al.* Structure-based design of prefusion-stabilized SARS-CoV-2 spikes. *Science* **369**, 1501-1505, doi:doi:10.1126/science.abd0826 (2020).

26 Cao, Y. *et al.* BA.2.12.1, BA.4 and BA.5 escape antibodies elicited by Omicron infection. *Nature* **608**, 593-602, doi:10.1038/s41586-022-04980-y (2022).

27 Arevalo, C. P. *et al.* Original antigenic sin priming of influenza virus hemagglutinin stalk antibodies. *Proceedings of the National Academy of Sciences* **117**, 17221-17227, doi:doi:10.1073/pnas.1920321117 (2020).

28 Gostic, K. M., Ambrose, M., Worobey, M. & Lloyd-Smith, J. O. Potent protection against H5N1 and H7N9 influenza via childhood hemagglutinin imprinting. *Science* **354**, 722-726, doi:doi:10.1126/science.aag1322 (2016).

29 Chen, X. *et al.* Protective effect of plasma neutralization from prior SARS-CoV-2 Omicron infection against BA.5 subvariant symptomatic reinfection. *The Lancet Regional Health - Western Pacific* **33**, 100758, doi:https://doi.org/10.1016/j.lanwpc.2023.100758 (2023).

30 Greaney, A. J. *et al.* Complete Mapping of Mutations to the SARS-CoV-2 Spike Receptor-

420 Binding Domain that Escape Antibody Recognition. *Cell Host Microbe* **29**, 44-57 e49,
421 doi:10.1016/j.chom.2020.11.007 (2021).
422 31 Cao, Y. *et al.* Omicron escapes the majority of existing SARS-CoV-2 neutralizing antibodies.
423 *Nature* **602**, 657-663, doi:10.1038/s41586-021-04385-3 (2022).
424 32 Starr, T. N. *et al.* SARS-CoV-2 RBD antibodies that maximize breadth and resistance to escape.
425 *Nature* **597**, 97-102, doi:10.1038/s41586-021-03807-6 (2021).
426 33 Cao, Y. *et al.* Rational identification of potent and broad sarbecovirus-neutralizing antibody
427 cocktails from SARS convalescents. *Cell Rep* **41**, 111845, doi:10.1016/j.celrep.2022.111845
428 (2022).
429 34 Barnes, C. O. *et al.* SARS-CoV-2 neutralizing antibody structures inform therapeutic strategies.
430 *Nature* **588**, 682-687, doi:10.1038/s41586-020-2852-1 (2020).
431 35 Corti, D., Purcell, L. A., Snell, G. & Veesler, D. Tackling COVID-19 with neutralizing
432 monoclonal antibodies. *Cell* **184**, 3086-3108, doi:10.1016/j.cell.2021.05.005 (2021).
433 36 Westendorf, K. *et al.* LY-CoV1404 (bebtelovimab) potently neutralizes SARS-CoV-2 variants.
434 *Cell Rep* **39**, 110812, doi:10.1016/j.celrep.2022.110812 (2022).
435 37 Mlcochova, P. *et al.* SARS-CoV-2 B.1.617.2 Delta variant replication and immune evasion.
436 *Nature* **599**, 114-119, doi:10.1038/s41586-021-03944-y (2021).
437 38 Addetia, A. *et al.* Therapeutic and vaccine-induced cross-reactive antibodies with effector
438 function against emerging Omicron variants. *bioRxiv*, 2023.2001.2017.523798,
439 doi:10.1101/2023.01.17.523798 (2023).
440 39 Hoffmann, M. *et al.* Effect of hybrid immunity and bivalent booster vaccination on omicron
441 sublineage neutralisation. *The Lancet Infectious Diseases* **23**, 25-28, doi:10.1016/S1473-
442 3099(22)00792-7 (2023).
443 40 Lim, W. W., Mak, L., Leung, G. M., Cowling, B. J. & Peiris, M. Comparative immunogenicity
444 of mRNA and inactivated vaccines against COVID-19. *The Lancet Microbe* **2**, e423,
445 doi:10.1016/S2666-5247(21)00177-4 (2021).

446 **Methods references**

447 41 Yanez Arteta, M. *et al.* Successful reprogramming of cellular protein production through mRNA
448 delivered by functionalized lipid nanoparticles. *Proceedings of the National Academy of*
449 *Sciences* **115**, E3351-E3360, doi:doi:10.1073/pnas.1720542115 (2018).
450 42 Starr, T. N. *et al.* Deep Mutational Scanning of SARS-CoV-2 Receptor Binding Domain Reveals
451 Constraints on Folding and ACE2 Binding. *Cell* **182**, 1295-1310 e1220,
452 doi:10.1016/j.cell.2020.08.012 (2020).
453 43 Otwinowski, J., McCandlish, D. M. & Plotkin, J. B. Inferring the shape of global epistasis. *Proc*
454 *Natl Acad Sci U S A* **115**, E7550-E7558, doi:10.1073/pnas.1804015115 (2018).
455 44 Traag, V. A., Waltman, L. & van Eck, N. J. From Louvain to Leiden: guaranteeing well-
456 connected communities. *Scientific Reports* **9**, 5233, doi:10.1038/s41598-019-41695-z (2019).
457 45 Starr, T. N. *et al.* Deep mutational scans for ACE2 binding, RBD expression, and antibody
458 escape in the SARS-CoV-2 Omicron BA.1 and BA.2 receptor-binding domains. *PLOS*
459 *Pathogens* **18**, e1010951, doi:10.1371/journal.ppat.1010951 (2022).
460 46 Bloom, J. D. & Neher, R. A. Fitness effects of mutations to SARS-CoV-2 proteins. *bioRxiv*,
461 2023.2001.2030.526314, doi:10.1101/2023.01.30.526314 (2023).

462

463 **Figure Legends**

464 **Fig. 1 | Humoral immune imprinting in mice.**

465 **a**, Neutralizing antibody response after priming with 2 doses of 3 μg CoronaVac followed by
466 boosting with 10 μg SARS-CoV-1 Spike protein or SARS-CoV-2 variant Spike proteins in mice. **b**,
467 Neutralizing antibody response after priming with 2 doses of 10 μg WT-mRNA followed by
468 boosting with 10 μg SARS-CoV-2 variant Spike proteins. **c**, Neutralizing antibody response after
469 immunization with 2 doses of 3 μg CoronaVac followed by boosting with 10 μg SARS-CoV-2
470 variant Spike proteins with 3 months or 6 months time interval in mice. **d**, Neutralizing antibody
471 response after priming with 2 doses of 3 μg CoronaVac followed by boosting twice with 10 μg
472 SARS-CoV-2 variant Spike proteins with different time intervals in mice. Mice were boosted twice
473 with intervals between boosters of either 1 month or 3 months. **e**, Neutralizing antibody response
474 after priming with 2 doses of 10 μg variant Spike proteins or 1 μg or 10 μg variant Spike mRNAs.
475 **f**, Neutralizing antibody response after priming with 2 doses of 3 μg CoronaVac followed by
476 boosting twice with 1 μg or 10 μg of SARS-CoV-2 variant Spike mRNAs. 10 mice were immunized
477 and analyzed in each group (n= 10). All Spike protein and mRNA contained six proline substitutions
478 (S6P) and alanine substitutions in the furin cleavage site to stabilize in prefusion conformation. The
479 time interval between the two priming doses is 2 weeks, unless stated otherwise. The interval
480 between priming and boosting is 4 weeks. Sera were collected one week after the last dose.
481 Geometric mean titers (GMT) were labeled. For paired samples in **a-d** and **f**, statistical significance
482 was determined using two-tailed Wilcoxon signed-rank tests. For independent samples in **e**,
483 statistical significance were determined using two-tailed Wilcoxon rank sum tests. *$p < 0.05$, **$p <$
484 0.01, and not significant (NS) $p > 0.05$. All neutralization assays were conducted in at least two
485 independent experiments.

486

487 **Fig. 2 | Humoral immune imprinting after repeated Omicron infections in humans.**

488 **a**, Examination of immune imprinting after Omicron breakthrough infections and repeated Omicron
489 infections. Plasma antibody titers against pseudotyped D614G and variants were measured. Fold
490 changes between titers against variants and D614G were calculated and shown above the line.
491 Statistical significance was determined using the Wilcoxon signed-rank test. BA.1, BA.2, BA.5,
492 BF.7 BTI: post-vaccination Omicron breakthrough infection (BTI). BA.1, BA.2 BTI+ BA.5/BF.7

493 infection: post-vaccination Omicron breakthrough infection followed by BA.5/BF.7 reinfection.
494 BA.1/BA.2+ BA.5/BF.7 infection: BA.1/BA.2 infection followed by BA.5/BF.7 reinfection with no
495 vaccination history. Blood samples were collected 1-2 months after the last infection. Detailed
496 information about the cohorts is in Supplementary Table 1. **b**, Plasma antibody breadth after
497 repeated Omicron infections. Plasma antibody titers against circulating pseudotyped variants were
498 measured. Fold changes between titers of different cohorts were calculated and shown above the
499 line. Statistical significance was determined using the Wilcoxon rank sum tests. **c**, Nasal swab
500 antibody breath after repeated Omicron infections. Nasal swab antibody titers against pseudotyped
501 variants were measured. Fold changes between titers of different cohorts were calculated and shown
502 above the line. Statistical significance was determined using the Wilcoxon rank sum test. Geometric
503 mean titers (GMT) are labeled in (**a**). Geometric mean ± SD are labeled in (**b, c**). Dashed lines
504 indicate the limit of detection (LOD, NT50 = 20). *$p < 0.05$, **$p < 0.01$, ***$p<0.001$,
505 ****$p<0.0001$, and not significant (NS) $p > 0.05$. All neutralization assays were conducted in at
506 least two independent experiments.
507
508 **Fig. 3 | B cell immune imprinting after repeated Omicron infections.**
509 **a–d**, Flow cytometry analysis of pooled B cells from Omicron infection convalescent individuals.
510 BA.1 (up) and BA.2 (down) RBD double-positive CD20+, IgM-, IgD-, CD27+ B cells were isolated
511 for paired-single-cell V(D)J sequencing. Flow cytometry analyses were performed in cohorts of the
512 following: (**a**) 2 months after BA.1 (up) or BA.2 (down) breakthrough infections, (**b**) 8 months after
513 BA.1 (up) or BA.2 (down) breakthrough infections, (**c**) 1 month after BA.5/BF.7 reinfection after
514 BA.1 (up) and BA.2 (down) breakthrough infections, **(d**) 2-3 months after BA.5/BF.7 reinfection
515 after BA.1 (up) or BA.2 (down) infection without SARS-CoV-2 vaccination history. APC,
516 allophycocyanine; FITC, fluorescein isothiocyanate; PE, phycoerythrin. BV605, Brilliant Violet
517 605. **e**, Proportions of WT-binding and non-WT-binding antibodies from Omicron breakthrough
518 infection and repeated Omicron infection cohorts. Binding specificity was determined by ELISA.
519 The antibodies were expressed in vitro using the sequence of the RBD-binding memory B cells from
520 various cohorts. **f**, The heavy-chain variable domain somatic hypermutation rate of the mAbs from
521 various cohorts. Statistical tests were determined using two-tailed Wilcoxon rank-sum tests. Boxes
522 display the 25th percentile, median and 75th percentile, and whiskers indicate median ± 1.5 times

523 the interquartile range. Violin plots show kernel density estimation curves of the distribution. The
524 numbers and ratios of samples in each group are labeled above the violin plots. *p < 0.05, **p <
525 0.01, ***p<0.001, ****p<0.0001, and not significant (NS) p > 0.05.
526
527 **Fig. 4 | Epitope distribution and characterization of mAbs elicited by Omicron BTI and**
528 **reinfection**
529 **a**, UMAP embedding of epitope groups of monoclonal antibodies (mAbs) binding BA.5 RBD
530 isolated from convalescent individuals who experienced BA.5/BF.7 BTI or reinfection (n=1350). **b**,
531 Neutralization activities, denoted as IC50 values, against SARS-CoV-2 D614G (n = 1349), BA.4/5
532 (n = 1322), and XBB.1.5 (n = 1346) spike-pseudotyped vesicular stomatitis viruses (VSV), as well
533 as ACE2 competition levels determined by ELISA (n = 1344), are projected onto the UMAP
534 embedding space. **c**, Distribution of mAbs across epitope groups is shown for BA.5 Breakthrough
535 Infection (BTI), BF.7 BTI, BA.1 BTI with reinfection, and BA.2 BTI with reinfection. Epitope
536 groups predominantly comprising non-neutralizing or weakly neutralizing mAbs (E2.2, E3, and F1)
537 are highlighted with dashed boxes. The percentage of antibodies in these three groups is labeled on
538 each bar. **d**, Average DMS escape scores of the crucial epitope groups contributing to neutralization
539 against XBB.1.5 are illustrated on the structure model of the SARS-CoV-2 BA.5 RBD (PDB:
540 7XNS). Key residues with high escape scores for each group are labeled. **e**, The average DMS
541 escape scores for the key epitope groups are represented as sequence logos; residues are depicted
542 using the standard one-letter code and colored based on their chemical properties. The height of
543 each letter corresponds to the escape score of the respective mutation. **f**, Pseudovirus-neutralization
544 activities of mAbs within the six crucial epitope groups (A1 [n = 170], A2 [n = 60], B [n = 33], F3
545 [n = 129], D3 [n = 155], and D4 [n = 80]) are shown against SARS-CoV-2 D614G, BA.5, BQ.1.1,
546 and XBB.1.5. Geometric mean IC50 values are displayed as bars and labeled above each group of
547 data points.
548
549 **Fig. 5 | Estimate the evolutionary trends of XBB.1.5 RBD from DMS profiles.**
550 Normalized average DMS escape scores weighted by IC50 against XBB.1.5 using DMS profiles of
551 mAbs from BA.5/BF.7 BTI (**a**), and mAbs from BA.5/BF.7 BTI and BA.1/BA.2 BTI with
552 BA.5/BF.7 reinfection (**b**). The impacts of each mutation on ACE2 binding and RBD expression,

553 and the codon constraints on each residue, are also considered (see Methods). Residues with high
554 estimated preferences are labeled, and their corresponding mutation scores are shown as logos.
555
556 **Fig. 6 | Combination of escape mutations evades XBB.1.5-neutralizing antibodies from**
557 **reinfection.**
558 **a**, SARS-CoV-2 XBB.1.5-based pseudoviruses harboring combinations of critical mutations
559 identified through analysis of DMS profiles are generated. **b**, hACE2-binding affinity for various
560 RBD mutants of SARS-CoV-2 is assessed using SPR. Geometric mean dissociation constants (KD)
561 from at least four independent replicates are shown, with statistical significance in comparison to
562 XBB.1.5 RBD's KD labeled above the bars. P-values are determined using a two-tailed t-test on
563 log-transformed KD values. **c**, IC50 values for representative potent XBB.1.5-neutralizing
564 antibodies from different epitope groups against XBB.1.5 variants carrying individual or multiple
565 escape mutations are displayed. Fold changes in IC50 against the mutants relative to XBB.1.5 are
566 presented as a heatmap. **d-f**, Pseudovirus 50% neutralization titers (NT50) for SARS-CoV-2
567 XBB.1.5-based mutants are shown using plasma from convalescent individuals who experienced
568 BA.5 or BF.7 reinfection: BA.1 BTI prior to BA.5/BF.7 reinfection (n = 26) (**d**); BA.2 BTI prior to
569 BA.5/BF.7 reinfection (n = 19) (**e**); and reinfection with BA.5 or BF.7 after BA.1 or BA.2 infection
570 without vaccination (n = 12) (**f**). Key mutations diminishing neutralization are labeled above their
571 corresponding lines. Dashed lines indicate the limit of detection (LOD, NT50 = 20). Geometric
572 mean titers are labeled above data points. Statistical tests are performed between neighboring
573 mutants. P-values are calculated using two-tailed Wilcoxon signed-rank tests on paired samples. *p
574 < 0.05, **p < 0.01, ***p<0.001, ****p<0.0001, and not significant (NS) p > 0.05.
575
576 **Methods**
577 **Isolation of PBMCs and plasma**
578 Blood samples from vaccinated or unvaccinated individuals who had recovered from Omicron
579 breakthrough infection or reinfection were obtained under study protocols approved by Beijing
580 Ditan Hospital, Capital Medical University (Ethics committee archiving No. LL-2021-024-02) and
581 the Tianjin Municipal Health Commission, and the Ethics Committee of Tianjin First Central
582 Hospital (Ethics committee archiving No. 2022N045KY). All participants have provided written

583 informed consent for the collection of information, storage and use of their clinical samples for
584 research purposes, and publication of data generated from this study.
585
586 The whole blood samples were 1:1 diluted with 2% fetal bovine serum (FBS) (Hyclone,
587 SH30406.05) in phosphate buffered saline (PBS) (Invitrogen, C10010500BT) and subjected to
588 Ficoll (Cytiva, 17-1440-03) gradient centrifugation to isolate plasma and PBMCs. Plasma was
589 collected from upper layer after centrifugation. PBMCs were collected at the interface and further
590 prepared through centrifugation, red blood cell lysis (Invitrogen™ eBioscience™ 1X RBC Lysis
591 Buffer, 00-4333-57) and washing steps. If not used for downstream process immediately, samples
592 were stored in FBS with 10% DMSO (Sigma-Aldrich, D4540) in liquid nitrogen. All PBMC
593 samples were shipped on dry ice and cryopreserved PBMCs were thawed in PBS + 1mM EDTA
594 (Invitrogen, AM9260G) + 2% FBS before use.
595
596 **mRNA vaccine preparation and mouse immunization**
597 For mRNA vaccine preparation, 5′ untranslated region (UTR), target sequence, and 3'UTR were
598 sequentially inserted after T7 promoter in an empty PSP73 plasmid firstly. The plasmid was then
599 subjected to double digestion to obtain linearized DNA. This DNA served as a template for an in
600 vitro transcription reaction mediated by T7 RNA polymerase to synthesize RNA encoding the
601 SARS-CoV-2 S6P (F817P, A892P, A899P, A942P, K986P, V987P, R683A and R685A) protein
602 according to the manufacturer's instructions (Vazyme, DD4201). Uridine was fully replaced by N1-
603 methyl-pseudouridine in this process. Transcription products were treated with DNase I to remove
604 DNA templates, and purified using VAHTS RNA Clean Beads (Vazyme, N412-02). Cap 1 structure
605 was added using Vaccinia Capping Enzyme (Vazyme, DD4109) and mRNA Cap 2'-O-
606 Methyltransferase (Vazyme, DD4110), followed by magnetic bead purification. Poly(A) tails were
607 added using E.coli Poly(A) Polymerase (Vazyme, N412-02) and the product was purified again.
608
609 The mRNA was encapsulated in a functionalized lipid nanoparticle as described previously[41]. In
610 brief, ionizable lipid, DSPC, cholesterol, and PEG2000-DMG were dissolved in ethanol at the mole
611 ratio of 50:10:38.5:1.5, respectively. mRNA was diluted in RNase free 50 mM citrate buffer (pH
612 4.0) to obtain a final lipid:mRNA weight ratio of 6:1. The aqueous and ethanol solutions were mixed

613 in a 3:1 volume ratio using a microfluidic apparatus and the obtained LNPs were dialyzed overnight.
614 All of the samples were stored within a week at 2~8 ℃ of use to ensure the chemical stability of the
615 components. The size of LNPs, the particle size distributions, and the encapsulation and
616 concentration of mRNA were determined. The encapsulation in all of the samples was typically 90–
617 99%.
618
619 Animal experiments were carried out under study protocols approved by Institute of Biophysics,
620 Chinese Academy of Sciences (SYXK2023300) and HFK Biologics (HFK-AP-20210930). Mice
621 were immunized according to schemes in figure 1. All inactivated vaccines were administered
622 intraperitoneally at a dose of 3 μg per mouse, while mRNA vaccines were administered
623 intramuscularly at a dose of 10 μg per mouse. Protein subunit vaccines were administered
624 subcutaneously at six sites on the back at a dose of 10 μg per mouse, where complete Freund's
625 adjuvant was used for the prime immunization, and incomplete Freund's adjuvant was used for
626 booster immunizations, with a 1:1 volume ratio of protein subunit and adjuvant. The second
627 immunizations were given 2 weeks after the first dose, with subsequent doses administered at 1-
628 month intervals, unless stated otherwise. Blood samples were collected 1 week after the final
629 immunization.
630
631 **BCR sequencing, analysis and recombinant antibody expression**
632 $CD19^+$ B cells were enriched from PBMCs using EasySep Human CD19 Positive Selection Kit II
633 (STEMCELL, 17854). Following enrichment, $1x10^6$ B cells in 100 μl buffer were incubated with a
634 panel of antibodies including 3 μl FITC anti-human CD20 antibody (BioLegend, 302304), 3.5 μl
635 Brilliant Violet 421 anti-human CD27 antibody (BioLegend, 302824), 2 μl PE/Cyanine7 anti-
636 human IgD antibody (BioLegend, 348210) and 2 μl PE/Cyanine7 anti-human IgM antibody
637 (BioLegend, 314532). Additionally, fluorophore or oligonucleotide conjugated RBD were added.
638 For FACS, 0.013 μg of biotinylated BA.1 (Sino Biological, 40592-V49H7-B) or BA.2 (customized
639 from Sino Biological) RBD protein conjugated with PE-streptavidin (BioLegend, 405204) and
640 APC-streptavidin (BioLegend, 405207), and 0.013 μg of WT biotinylated RBD protein (Sino
641 Biological, 40592-V27H-B) conjugated with BV605-streptavidin (BioLegend, 405229) were added.
642 For sequencing, BA.1 or BA.2 biotinylated RBD protein conjugated with TotalSeq™-C0971

643 Streptavidin (BioLegend, 405271) and TotalSeq™-C0972 Streptavidin (BioLegend, 405273), WT
644 biotinylated RBD protein conjugated with TotalSeq™-C0973 Streptavidin (BioLegend, 405275)
645 and TotalSeq™-C0974 Streptavidin (BioLegend, 405277) and biotinylated Ovalbumin (Sino
646 Biological) conjugated with TotalSeq™-C0975 Streptavidin (BioLegend, 405279) were added.
647 After incubation and washing steps, 5 µl of 7-AAD (Invitrogen, 00-6993-50) was included for dead
648 cell exclusion.
649
650 Cells negative for 7-AAD, IgM and IgD, but positive for CD20, CD27 and BA.1 or BA.2 were
651 sorted using a MoFlo Astrios EQ Cell Sorter (Beckman Coulter). FACS data were collected by
652 Summit 6.0 (Beckman Coulter) and analyzed using FlowJo v10.8 (BD Biosciences).
653
654 The sorted B cells were processed using the Chromium Next GEM Single Cell V(D)J Reagent Kits
655 v1.1 according to the manufacturer's user guide (10x Genomics, CG000208). Briefly, the cells were
656 resuspended in PBS after centrifugation and then processed to obtain gel beads-in-emulsion (GEMs)
657 using the 10X Chromium controller. The GEMs were subjected to reverse transcription and the
658 products were further purified with a GEM-RT clean up procedure. Preamplification was then
659 performed on the products which were subsequently purified using the SPRIselect Reagent Kit
660 (Beckman Coulter, B23318). The paired V(D)J BCR sequences were enriched with 10X BCR
661 primers, followed by library preparation. Finally, the libraries were sequenced using the Novaseq
662 6000 platform, running either the Novaseq 6000 S4 Reagent Kit v1.5300 cycles (Illumina,
663 20028312) or the NovaSeq XP 4-Lane Kit v1.5 (Illumina, 20043131).
664
665 10X Genomics V(D)J sequencing data were assembled as BCR contigs and aligned using the Cell
666 Ranger (v6.1.1) pipeline according to the GRCh38 BCR reference. To ensure high quality, only the
667 productive BCR contigs and cells with one heavy chain and one light chain were retained. The
668 IgBlast program (v1.17.1) was utilized to identify and annotate the germline V(D)J genes. The
669 Change-O toolkit (v1.2.0) was employed to detect somatic hypermutation sites in the variable
670 domain of the antibodies.
671
672 For expression optimization in human cells, heavy and light chain genes were synthesized by

673 GenScript, inserted separately into plasmids (pCMV3-CH, pCMV3-CL or pCMV3-CK) via
674 infusion (Vazyme, C112), and co-transfected into Expi293F cells (Thermo Fisher, A14527) using
675 polyethylenimine transfection. The cells were cultured at 36.5°C in 5% CO_2 and 175 r.p.m. for 6-
676 10 days. The cell expression fluid was collected and centrifuged. After centrifugation, supernatants
677 containing the monoclonal antibodies were purified using protein A magnetic beads (L00695,
678 Genscript). The purified samples were determined by SDS-PAGE.
679
680 **Pseudovirus-neutralization assay**
681 Codon-optimized SARS-CoV-2 S gene was inserted into the pcDNA3.1 vector to construct
682 plasmids encoding the spike proteins of SARS-CoV-2 and G*ΔG-VSV was amplified before
683 production of SARS-CoV-2 pseudotyped virus. The 293T cell line (ATCC, CRL-3216) was infected
684 with G*ΔG-VSV virus (VSV G pseudotyped virus, Kerafast) and transfected with the spike protein-
685 expressing plasmids simultaneously. After culturing, the pseudovirus-containing supernatant was
686 collected, filtered, aliquoted, and frozen at −80 °C for future use. Pseudovirus-neutralization assays
687 were conducted on the Huh-7 cell line (Japanese Collection of Research Bioresources (JCRB),
688 0403).
689
690 Monoclonal antibodies or plasma were serially diluted in DMEM (Hyclone, SH30243.01) and
691 incubated with pseudovirus in 96-well plates at 5% CO_2 and 37°C for 1 h. Digested Huh-7 cell
692 (JCRB, 0403) or 293T-hACE2 cells (ATCC, CRL-3216) were seeded and cultured for 24h. Half of
693 the supernatant was then discarded and D-luciferin reagent (PerkinElmer, 6066769) was added to
694 react in the dark. The luminescence value was detected using a microplate spectrophotometer
695 (PerkinElmer, HH3400). IC50 was determined by a four-parameter logistic regression model using
696 PRISM (version 9.0.1).
697
698 **ELISA**
699 ELISA assays were conducted by pre-coating ELISA plates with RBD (SARS-CoV-2 wild type,
700 SARS-CoV-2 BA.1, SARS-CoV-2 BA.2 RBD, Sino Biological) at concentrations of 0.03 μg ml^{-1}
701 and 1 μg ml^{-1} in PBS overnight at 4 °C. The plates were then washed and blocked, after which 100 μl
702 of 1 μg ml^{-1} antibodies were added to each well and incubated at room temperature for 2 hours.

703 Following incubation, the plates were washed and incubated with 0.25 μg ml^{-1} Peroxidase-
704 conjugated AffiniPure goat anti-human IgG (H+L) (JACKSON, 109-035-003) for 1 hour at room
705 temperature. The reaction was developed using tetramethylbenzidine (TMB) (Solarbio, 54827-17-
706 7), and stopped by adding H_2SO_4. The absorbance was measured at 450 nm using a microplate
707 reader (PerkinElmer, HH3400) and the negative control used was the H7N9 human IgG1 antibody
708 HG1K. (Sino Biological, HG1K).
709
710 **Surface plasmon resonance**
711 Human ACE2 with Fc tag was immobilized onto Protein A sensor chips using a Biacore 8K (GE
712 Healthcare). Purified SARS-CoV-2 mutants RBD were prepared in serial dilutions, ranging from
713 100 to 6.25 nM, and injected over the sensor chips. The response units were recorded at room
714 temperature using BIAcore 8K Evaluation Software (v3.0.12.15655; GE Healthcare). The obtained
715 data were then analyzed using BIAcore 8K Evaluation Software (v3.0.12.15655; GE Healthcare)
716 and fitted to a 1:1 binding model.
717
718 **DMS Library construction**
719 Duplicate single site saturated mutant libraries spanning all 201 amino acids of BA.5 RBD (position
720 N331-T531 by Wuhan-Hu-1 reference numbering) were constructed based on previously reported
721 method[1], in order to ensure the reproducibility and reliability of results. A unique N26 barcode was
722 PCR appended to each RBD variant as an identifier, and the correspondence of variant and N26
723 barcode was obtained by PacBio sequencing on Sequel ll platform in Peking University throughput
724 sequencing center (HTSC). The BA.5 RBD mutant libraries were assembled into pETcon 2649
725 vector and amplified in DH10B cells. Above plasmids products were then transformed into
726 Saccharomyces cerevisiae EBY100. Yeasts were screened on SD-CAA plates and further enlarged
727 in SD-CAA liquid media, the resulted libraries were preserved at -80°C after flash frozen in liquid
728 nitrogen.
729
730 **MACS-based mutation escape profiling**
731 The high-throughput mutation escape profiling for every single antibody was performed as
732 previously described[7,26]. Briefly, unexpressed and non-functional RBD variants were first

733 eliminated from BA.5 mutant libraries by magnetic-activated cell sorting (MACS). The selected
734 yeasts were inoculated into SG-CAA media to induce RBD surface expression by overnight culture.
735 To capture yeast cells that escape specific antibody binding, two rounds of sequential negative
736 selection and one round of positive selection were carried out based on MACS. After overnight
737 amplification, plasmids were extracted from the sorted yeasts using the 96 Well Plate Yeast Plasmid
738 Preps Kit (Coolaber, PE053), then used as template for N26 barcode amplification by PCR. Final
739 PCR products were purified, quantified, and sequenced on Nextseq 550 or MGISEQ-2000 platform.
740

741 **DMS data analysis and antibody clustering**

742 DMS raw sequencing data were processed as described previously[7,26]. In brief, the detected barcode
743 sequences of both the antibody-screened and reference library were aligned to the barcode-variant
744 dictionary generated using dms_variants (v0.8.9) from PacBio sequencing data of the BA.5 DMS
745 library. Only barcodes that are detected more than 5 times in the reference library are included in
746 the calculation to avoid large sampling error. The escape scores of a variant X that are detected both
747 in the screened and reference library were defined as $F\times(n_{X,ab} / N_{ab}) / (n_{X,ref} / N_{ref})$, where F is a scale
748 factor to normalize the scores to the 0-1 range, while n and N are the number of detected barcodes
749 for variant X and total barcodes in antibody-screened (ab) or reference (ref) samples, respectively.
750 To assign an escape score to each single substitution on RBD, an epistasis model is fitted using
751 dms_variants (v0.8.9) as described previously[42,43]. For antibodies with multiple replicates of DMS,
752 the final escape score of each mutation is the average over all replicates.

753 We used graph-based unsupervised clustering and embedding to assign an epitope group for each
754 antibody and visualize them in a two-dimensional space. First, site escape scores (the sum of
755 mutation escape scores on a residue) of each antibody are first normalized to a sum of one and
756 considered as a distribution over RBD residues. The dissimilarity of two antibodies is defined by
757 the Jessen-Shannon divergence of the normalized escape scores. Pair-wise dissimilarities of all
758 antibodies in the dataset are calculated using the SciPy module
759 (scipy.spatial.distance.jensenshannon, v1.7.0). Then, a 12-nearest-neighbor graph is built using
760 python-igraph module (v0.9.6). Leiden clustering is performed to assign a cluster to each antibody
761 [44]. The name of each cluster is annotated manually based on the featured sites on the average escape

762 profiles of a cluster to make it consistent with the definition of our previously published DMS
763 dataset using WT-based library in general[7]. To project the dataset onto a 2D space for visualization,
764 we performed UMAP based on the constructed k-nearest-neighbor graph using umap-learn module
765 (v0.5.2). Figures were generated by R package ggplot2 (v3.3.3).

766 **Estimate the preference of RBD mutations**

767 Similar to the approach in our previous study[7], we incorporated four types of weights in our
768 calculations to account for the impact of each mutation on hACE2-binding affinity, RBD expression,
769 neutralizing activity, and the codon constraints on each residue. The weights for ACE2 binding and
770 RBD expression are determined by $\tanh(S_{\mathrm{bind}}) + 1$ and $\tanh\big(\min\big(0, S_{\mathrm{expr}}\big)\big) + 1$, respectively,
771 where the $\mathrm{S}_{\mathrm{bind}}$ and $\mathrm{S}_{\mathrm{expr}}$ values are from the BA.2-based DMS on ACE2 binding and RBD
772 expression[45]. The function $\tanh(x)$ is employed as a sigmoidal curve to constrain the weights
773 between 0 and 2. For codon constraint weights, mutations that cannot be accessed through single
774 nucleotide mutation are first assigned a weight of zero. To address the intrinsic disparities in the
775 frequency of distinct nucleotide substitutions in SARS-CoV-2, we assign different weights for
776 mutations corresponding to various nucleotide substitutions[46]. Specifically, the weight of the most
777 frequent substitution (C>T) is assigned a value of 0.1, while weights for G>T and G>A are 0.041
778 and 0.035, respectively. To retain the potential of rare mutations, all other substitutions are assigned
779 a weight of 0.03. We use BA.4/5 (EPI_ISL_11207535) and XBB.1.5 (EPI_ISL_17054053) to define
780 weights for codon usage. Regarding the neutralizing activities, the weight is calculated as -
781 $\log_{10}(\mathrm{IC}_{50})$. IC_{50} values (μg/mL) less than 0.0005 or greater than 1.0 are considered as 0.0005 or 1.0,
782 respectively. As the dataset specifically enriches for Omicron-specific antibodies, potentially
783 introducing bias when estimating mutation preferences. An additional weighting strategy is applied
784 that assigns higher weights to cross-reactive mAbs, resulting in 89% cross-reactive mAbs for
785 BA.5/BF.7 BTI cohorts and 51% for reinfection cohorts, as determined by unbiased characterization
786 of mAbs using ELISA. The raw escape scores for each antibody are first normalized by the
787 maximum score among all mutants. The weighted score for each antibody and each mutation is
788 obtained by multiplying the normalized scores with the corresponding four weights, and the final
789 mutation-specific weighted score is the sum of scores for all antibodies in the designated set, which
790 is then normalized once more to produce a value between 0 and 1. To visualize the calculated escape

maps, sequence logos were created using the Python module logomaker (v0.8).

Methods references

41 Yanez Arteta, M. *et al.* Successful reprogramming of cellular protein production through mRNA delivered by functionalized lipid nanoparticles. *Proceedings of the National Academy of Sciences* **115**, E3351-E3360 (2018). https://doi.org:doi:10.1073/pnas.1720542115

42 Starr, T. N. *et al.* Deep Mutational Scanning of SARS-CoV-2 Receptor Binding Domain Reveals Constraints on Folding and ACE2 Binding. *Cell* **182**, 1295-1310 e1220 (2020). https://doi.org:10.1016/j.cell.2020.08.012

43 Otwinowski, J., McCandlish, D. M. & Plotkin, J. B. Inferring the shape of global epistasis. *Proc Natl Acad Sci U S A* **115**, E7550-E7558 (2018). https://doi.org:10.1073/pnas.1804015115

44 Traag, V. A., Waltman, L. & van Eck, N. J. From Louvain to Leiden: guaranteeing well-connected communities. *Scientific Reports* **9**, 5233 (2019). https://doi.org:10.1038/s41598-019-41695-z

45 Starr, T. N. *et al.* Deep mutational scans for ACE2 binding, RBD expression, and antibody escape in the SARS-CoV-2 Omicron BA.1 and BA.2 receptor-binding domains. *PLOS Pathogens* **18**, e1010951 (2022). https://doi.org:10.1371/journal.ppat.1010951

46 Bloom, J. D. & Neher, R. A. Fitness effects of mutations to SARS-CoV-2 proteins. *bioRxiv*, 2023.2001.2030.526314 (2023). https://doi.org:10.1101/2023.01.30.526314

Acknowledgments

We would like to express our gratitude to Jesse D. Bloom and Tyler N. Starr for their invaluable insights and discussions during the construction of our deep mutation scanning libraries. We thank all volunteers for providing the blood samples. We gratefully acknowledge the assistance of the High-throughput Sequencing Center at Peking University and Annoroad Gene Technology Co., Ltd. in sample sequencing. This project is financially supported by the Ministry of Science and Technology of China and Changping Laboratory (2021A0201; 2021D0102), and National Natural Science Foundation of China (32222030).

Author contributions

Y.C. designed and supervised the study. A.Y., F.J., W.S., Q.G., X.S.X, and Y.C. wrote the manuscript with inputs from all authors. A.Y., W.S., S.Y., R.A., Yao W., and X.N. performed B-cell sorting, single-cell VDJ sequencing, and antibody sequence analyses. J.W. (BIOPIC), F.J., H.S. and L.Z.

824 performed and analyzed the DMS data. Y.Y. and Youchun W. constructed the pseudotyped virus.
825 N.Z., P.W., L.Y., T.X. and F.S. performed the pseudotyped virus neutralization assays. W.S. and A.Y.
826 analyzed the neutralization data. Y.X., X.C., Z.S. and R.J. recruited the SARS-CoV-2 vaccinees and
827 convalescents. J.W. (Changping Laboratory), L.Y. and F.S. performed the antibody expression.
828

829 **Conflicts of interest**

830 X.S.X. and Y.C. are inventors on the provisional patent applications of BD series antibodies, which
831 include BD55-5514 (SA55) and mAbs from Omicron infection convalescents. X.S.X. and Y.C. are
832 founders of Singlomics Biopharmaceuticals. Other authors declare no competing interests.

833 **Data and code availability**

834 Information of SARS-CoV-2 RBD-targeting mAbs is included in Supplementary Table 2. Processed
835 mutation escape scores, and custom scripts for processing and analyzing DMS data can be
836 downloaded at https://github.com/jianfcpku/SARS-CoV-2-reinfection-DMS. Raw sequencing data
837 of DMS are available on China National GeneBank with Project accession CNP0004294. PDB
838 7XNS is used for the structural model of SARS-CoV-2 RBD.
839

840 **Extended Data Figure Legends**

841

842 **Extended Data Fig. 1 | Neutralizing antibody response after CoronaVac primary and spike**
843 **protein booster**

844 **a**, Comparison of neutralizing antibody responses among mouse immunization groups against
845 pseudotyped D614G, SARS, and additional SARS-CoV-2 variants. Mice sera antibody titers after
846 priming with two doses of 3 μg CoronaVac followed by boosting with 10 μg SARS-CoV-1 Spike
847 protein or SARS-CoV-2 variant Spike proteins in mice, or no boosting were measured. Fold changes
848 between groups receiving different boosters and the primary-only group were calculated and shown
849 above the line. Statistical significance was determined using the Wilcoxon rank sum test. **b**,
850 Antibody breadth after priming with CoronaVac followed by boosting with different Spike proteins
851 or no boosting. The neutralizing titer data used is the same as in a. Fold changes between titers
852 against SARS or SARS-CoV-2 variants, and D614G were calculated and shown above the line.

853 Statistical significance was determined using the Wilcoxon signed-rank test. *p < 0.05, **p < 0.01,
854 ***p<0.001, ****p<0.0001, and not significant (NS) p > 0.05.
855
856 **Extended Data Fig. 2 | Neutralizing antibody response with mRNA vaccine as primary or**
857 **booster**
858 **a**, Comparison of neutralizing antibody responses among mouse immunization groups against
859 pseudotyped D614G, SARS, and additional SARS-CoV-2 variants. Mice sera antibody titers after
860 priming with 2 doses of 10 μg WT-mRNA followed by boosting with 10 μg SARS-CoV-2 variant
861 Spike proteins in mice, or no boosting were measured. Fold changes between groups receiving
862 different boosters and the primary-only group were calculated and shown above the line. Statistical
863 significance was determined using the Wilcoxon rank sum test. **b**, Antibody breadth after priming
864 with WT-mRNA followed by boosting with SARS-CoV-2 variant Spike proteins in mice, or no
865 boosting. The neutralizing titer data used is the same as in a. Fold changes between titers against
866 SARS or SARS-CoV-2 variants, and D614G were calculated and shown above the line. Statistical
867 significance was determined using the Wilcoxon signed-rank test. Fold changes between titers
868 against SARS or SARS-CoV-2 variants and D614G were calculated and shown above the line.
869 Statistical significance was determined using the Wilcoxon signed-rank test. *p < 0.05, **p < 0.01,
870 ***p<0.001, ****p<0.0001, and not significant (NS) p > 0.05.
871
872 **Extended Data Fig. 3 | Comparison of neutralizing antibody responses with different intervals**
873 **between the first and second Spike protein boosters.**
874 **a,** Comparison of neutralizing antibody responses among different groups of mice immunized with
875 2 doses of CoronaVac, followed by two BA.5/BQ.1.1/XBB Spike protein boosters administered
876 with one-month or three-month intervals between the first and second boosters, and compared to
877 the primary immunization. Statistical significance was determined using the Wilcoxon rank sum
878 test. **b,** Antibody breadth after priming with CoronaVac followed by boosting with 2 doses of
879 BA.5/BQ.1.1/XBB Spike proteins with a one-month interval between the first and second boosters.
880 Statistical significance was determined using the Wilcoxon signed-rank test. **c,** Antibody breadth
881 after priming with 2 doses of BA.5/BQ.1.1/XBB Spike proteins. Statistical significance was
882 determined using the Wilcoxon signed-rank test. **d,** Antibody breadth after priming with CoronaVac

883 followed by boosting with 2 doses of BA.5/BQ.1.1/XBB Spike proteins with a three-month interval
884 between the first and second boosters. Statistical significance was determined using the Wilcoxon
885 signed-rank test. *p < 0.05, **p < 0.01, ***p<0.001, ****p<0.0001, and not significant (NS) p >
886 0.05.
887
888 **Extended Data Fig. 4 | Comparison of neutralizing antibody responses with different intervals**
889 **between primary vaccination and the first booster.**
890 **a,** Comparison of neutralizing antibody responses among different groups of mice immunized with
891 2 doses of CoronaVac, followed by two additional doses of SARS-CoV-2 Spike protein vaccine at
892 different intervals. Statistical significance was determined using the Wilcoxon signed-rank test. **b-**
893 **c,** Comparison of neutralizing antibody responses among different groups of mice immunized with
894 2 doses of CoronaVac, followed by one dose of BQ.1.1(b) or XBB(c) Spike protein vaccine at
895 different intervals. Statistical significance was determined using the Wilcoxon rank sum test. **d-e,**
896 Comparison of neutralizing antibody responses among different groups of mice immunized with 2
897 doses of CoronaVac, followed by two additional doses of BQ.1.1(d) or XBB(e) Spike protein
898 vaccine at different intervals. Statistical significance was determined using the Wilcoxon rank sum
899 test. *p < 0.05, **p < 0.01, ***p<0.001, ****p<0.0001, and not significant (NS) p > 0.05.
900
901 **Extended Data Fig. 5 | Comparison of neutralizing antibody responses with different mRNA**
902 **vaccine booster dosages.**
903 **a-b,** Antibody breadth after priming with 2 doses of 3 μg CoronaVac followed by boosting with 1
904 dose of 1μg (a) or 10μg (b) BA.5/BQ.1.1/XBB Spike proteins in mice. Statistical significance was
905 determined using the Wilcoxon signed-rank test. **c-d,** Antibody breadth after priming with 2 doses
906 of 3 μg CoronaVac followed by boosting with 2 doses of 1μg (c) or 10μg (d) BA.5/BQ.1.1/XBB
907 Spike proteins in mice. Statistical significance was determined using the Wilcoxon signed-rank test.
908 **e,** Comparison of neutralizing antibody responses among different groups of mice immunized with
909 2 doses of CoronaVac, followed by 2 doses of BA.5/BQ.1.1/XBB mRNA boosters at different doses
910 and compared to the primary immunization. Statistical significance was determined using the
911 Wilcoxon rank sum test. *p < 0.05, **p < 0.01, ***p<0.001, ****p<0.0001, and not significant (NS)
912 p > 0.05.

913

914 **Extended Data Fig. 6 | Antibody breadth of plasma and nasal swab after repeated Omicron**
915 **infections.**

916 **a-c**, Plasma antibody titers against pseudotyped D614G and variants after (a) BA.1 BTI + BA.5/BF.7
917 infection (n = 26), (b) BA.2 BTI + BA.5/BF.7 infection (n = 19), (c) BA.1/BA.2 + BA.5 infection
918 (n = 12). Fold changes between titers against variants and D614G were calculated and shown above
919 the line. Statistical significance was determined using the Wilcoxon signed-rank test.

920 **d-f**, Nasal swab antibody titers against pseudotyped D614G and variants after (d) BA.1 BTI +
921 BA.5/BF.7 infection (n = 26), (e) BA.2 BTI + BA.5/BF.7 infection (n = 19), (f) BA.1/BA.2 + BA.5
922 infection (n = 12). Fold changes between titers against variants and D614G were calculated and
923 shown above the line. Statistical significance was determined using the Wilcoxon signed-rank test.
924 *p < 0.05, **p < 0.01, ***p<0.001, ****p<0.0001, and not significant (NS) p > 0.05.

925

926 **Extended Data Fig. 7 | Characteristics of BA.5-reactive mAbs elicited by BA.5/BF.7 BTI or**
927 **reinfection.**

928 **a,** Source of the antibodies are projected onto the UMAP embedding space. Antibodies from BA.5
929 BTI (n=445), BF.7 BTI (n=243), BA.1 BTI with reinfection (n=284), and BA.2 BTI with reinfection
930 (n=232) are colored blue in the corresponding panel, and other antibodies are gray. **b**, Neutralization
931 activities, denoted as IC50 values, against SARS-CoV-2 BA.1 (n = 1260), BA.2 (n = 1238), BA.2.75
932 (n=1238), BQ.1.1 (n = 1335) and XBB (n = 1341) spike-pseudotyped VSV are projected onto the
933 UMAP embedding space. **c**, Average escape scores of epitope groups that are not shown in Fig. 4d
934 (C/D1, D2, E1/E2.1, E2.2, E3, and F1) are illustrated on the structure model of the SARS-CoV-2
935 BA.5 RBD (PDB: 7XNS). Key residues with high escape scores for each group are labeled. **d**,
936 Average DMS escape scores for these epitope groups are represented as sequence logos; residues
937 are depicted using the standard one-letter code and colored based on their chemical properties. The
938 height of each letter corresponds to the escape score of the respective mutation. **e**, Pseudovirus-
939 neutralization activities of XBB.1.5-neutralizing mAbs in groups A1 (n=70) and A2 (n=23) against
940 XBB.1.5 and XBB.1.5.10; and mAbs in groups B (n=15) and C/D1 (n=13) against XBB.1.5 and
941 XBB.1.16. Fold changes in IC50 are labeled. P-values are calculated using two-tailed Wilcoxon
942 signed-rank test of paired samples. **f,** Pseudovirus-neutralization activities of mAbs within the six

943 crucial epitope groups (C/D1 [n = 76], D2 [n = 86], E1/E2.1 [n = 100], E2.2 [n = 124], E3 [n = 101],
944 and F1 [n = 236]) are shown against SARS-CoV-2 D614G, BA.5, BQ.1.1, and XBB.1.5. Geometric
945 mean IC50 values are displayed as bars and labeled above each group of data points.
946
947 **Extended Data Fig. 8 | Workflow of calculating weighted escape scores of each mutation on**
948 **RBD.**
949 Weights for ACE2 binding and RBD expression, neutralization activity, and codon usage are
950 sequentially applied on the calculation to achieve informative results. Mutation preferences of BA.5
951 RBD under the pressure of NAbs from BA.5 or BF.7 BTI are shown.
952
953 **Extended Data Fig. 9 | SPR sensorgrams for affinity of hACE2 and SARS-CoV-2 mutants**
954 **RBD**
955 Representative sensorgram of at least four replicates is shown for each RBD. Geometric mean
956 kinetic constants k_a, k_d, and dissociation equilibrium constant K_D are labeled in each panel.
957
958 **Extended Data Fig. 10 | NAbs from BTI and reinfection are escaped by constructed mutants**
959 **a**, IC50 values for representative potent XBB.1.5-neutralizing antibodies from different epitope
960 groups against XBB.1.5 variants carrying individual or multiple escape mutations are shown. The
961 order of antibodies is the same as that in Fig. 6c. **b**, Pseudovirus NT50 for SARS-CoV-2 XBB.1.5-
962 based mutants are shown using plasma from convalescent individuals who experienced BA.5 (n=36)
963 or BF.7 BTI (n = 30). Statistical tests are performed between neighboring mutants. P-values are
964 calculated using two-tailed Wilcoxon signed-rank tests on paired samples. *$p < 0.05$, **$p < 0.01$,
965 ****$p < 0.0001$, and $p > 0.05$ (NS).
966
967

Figure 1

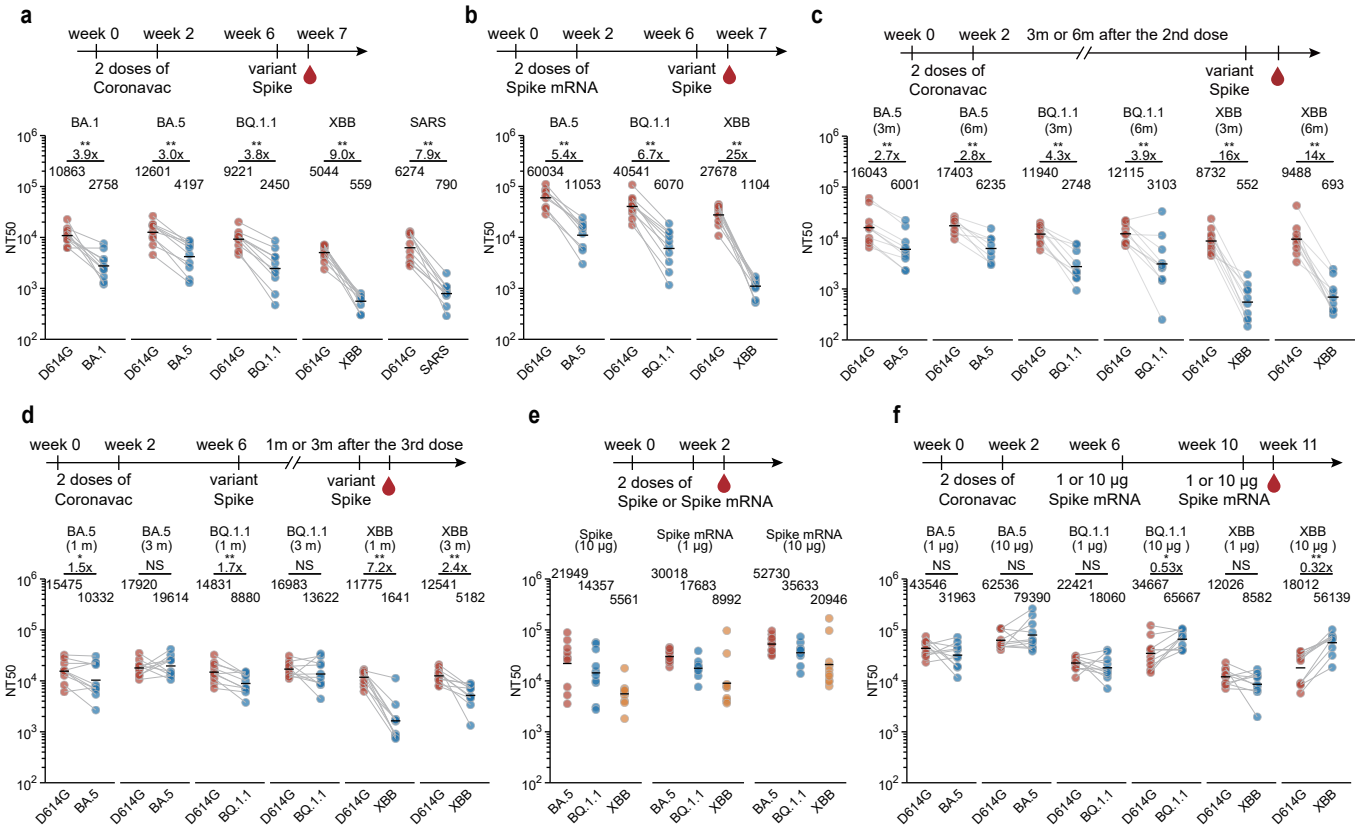

Fig.1| Humoral immune imprinting in mice.

a, Neutralizing antibody response after priming with 2 doses of 3 μg CoronaVac followed by boosting with 10 μg SARS-CoV-1 Spike protein or SARS-CoV-2 variant Spike proteins in mice. b, Neutralizing antibody response after priming with 2 doses of 10 μg WT-mRNA followed by boosting with 10 μg SARS-CoV-2 variant Spike proteins. c, Neutralizing antibody response after immunization with 2 doses of 3 μg CoronaVac followed by boosting with 10 μg SARS-CoV-2 variant Spike proteins with 3 months or 6 months time interval in mice. d, Neutralizing antibody response after priming with 2 doses of 3 μg CoronaVac followed by boosting twice with 10 μg SARS-CoV-2 variant Spike proteins with different time intervals in mice. Mice were boosted twice with intervals between boosters of either 1 month or 3 months. e, Neutralizing antibody response after priming with 2 doses of 10 μg variant Spike proteins or 1 μg or 10 μg variant Spike mRNAs. f, Neutralizing antibody response after priming with 2 doses of 3 μg CoronaVac followed by boosting twice with 1 μg or 10 μg of SARS-CoV-2 variant Spike mRNAs. 10 mice were immunized and analyzed in each group (n= 10). All Spike protein and mRNA used S6P prefusion-stabilization. The time interval between the two priming doses is 2 weeks. The interval between priming and boosting is 4 weeks. Sera were collected one week after the last dose. Geometric mean titers (GMT) were labeled. For paired samples in a-d and f, statistical significance were determined using two-tailed Wilcoxon signed-rank tests. For independent samples in e, statistical significance were determined using two-tailed Wilcoxon rank sum tests. *$p < 0.05$, **$p < 0.01$, and not significant (NS) $p > 0.05$. All neutralization assays were conducted in at least two independent experiments.

Figure 2

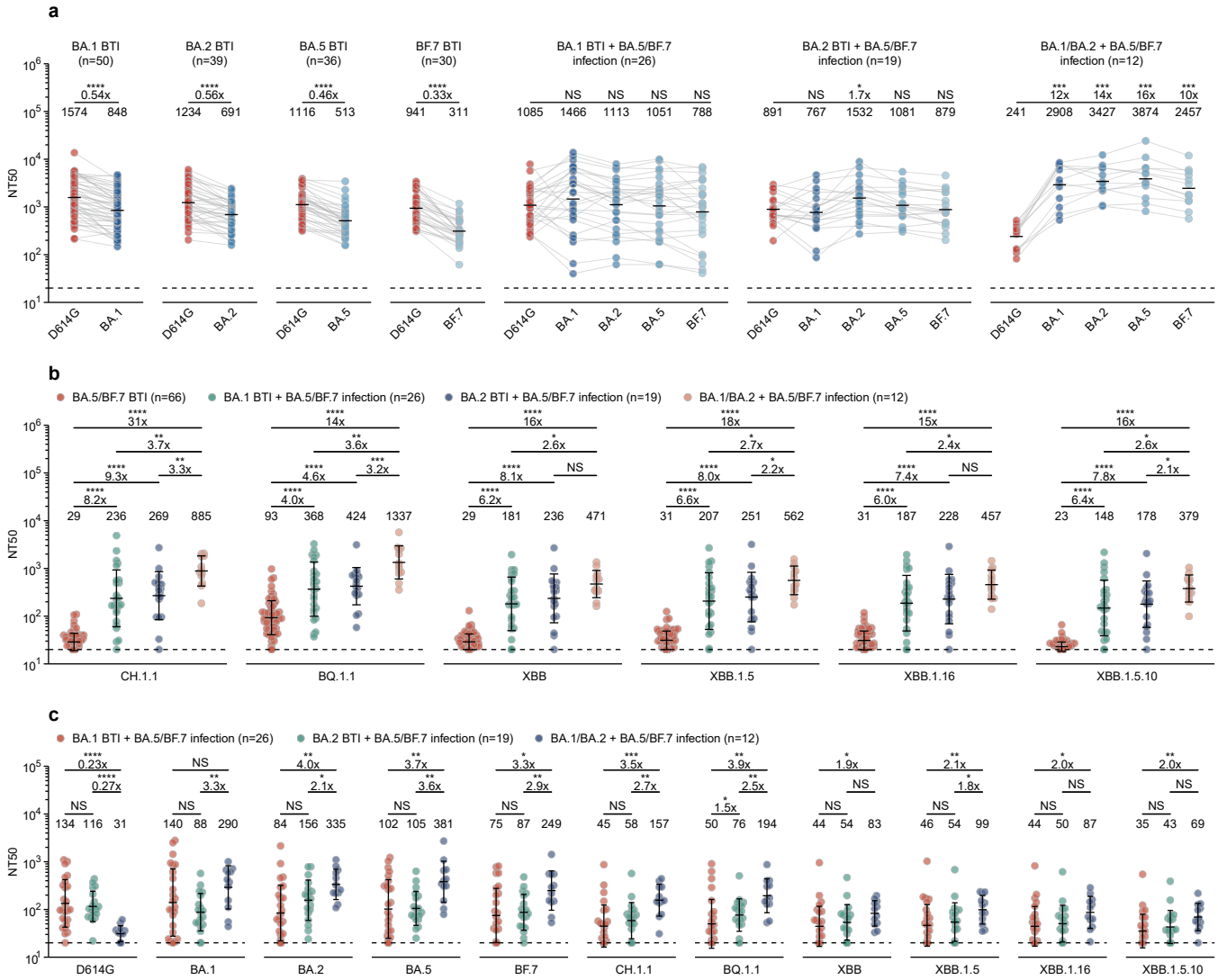

Fig.2| Humoral immune imprinting after repeated Omicron infections in human.
a, Examination of immune imprinting after Omicron breakthrough infections and repeated Omicron infections. Plasma antibody titers against pseudotyped D614G and variants were measured. Fold changes between titers against variants and D614G were calculated and shown above the line. Statistical significance was determined using the Wilcoxon signed-rank test. BA.1, BA.2, BA.5, BF.7 BTI: post-vaccination Omicron breakthrough infection (BTI). BA.1, BA.2 BTI+ BA.5/BF.7 infection: post-vaccination Omicron breakthrough infection followed by BA.5/BF.7 reinfection. BA.1/BA.2+ BA.5/BF.7 infection: BA.1/BA.2 infection followed by BA.5/BF.7 reinfection with no vaccination history. Blood samples were collected 1-2 months after the last infection. Detailed information about the cohorts is in Supplementary Table 1. b, Plasma antibody breadth after repeated Omicron infections. Plasma antibody titers against circulating pseudotyped variants were measured. Fold changes between titers of different cohorts were calculated and shown above the line. Statistical significance was determined using the Wilcoxon rank sum tests. c, Nasal swab antibody breath after repeated Omicron infections. Nasal swab antibody titers against pseudotyped variants were measured. Fold changes between titers of different cohorts were calculated and shown above the line. Statistical significance was determined using the Wilcoxon rank sum test. Geometric mean titers (GMT) are labeled in (a). Geometric mean ± SD are labeled in (b, c). Dashed lines indicate the limit of detection (LOD, NT50 = 20). *p < 0.05, **p < 0.01, ***p<0.001, ****p<0.0001, and not significant (NS) p > 0.05. All neutralization assays were conducted in at least two independent experiments.

Figure 3

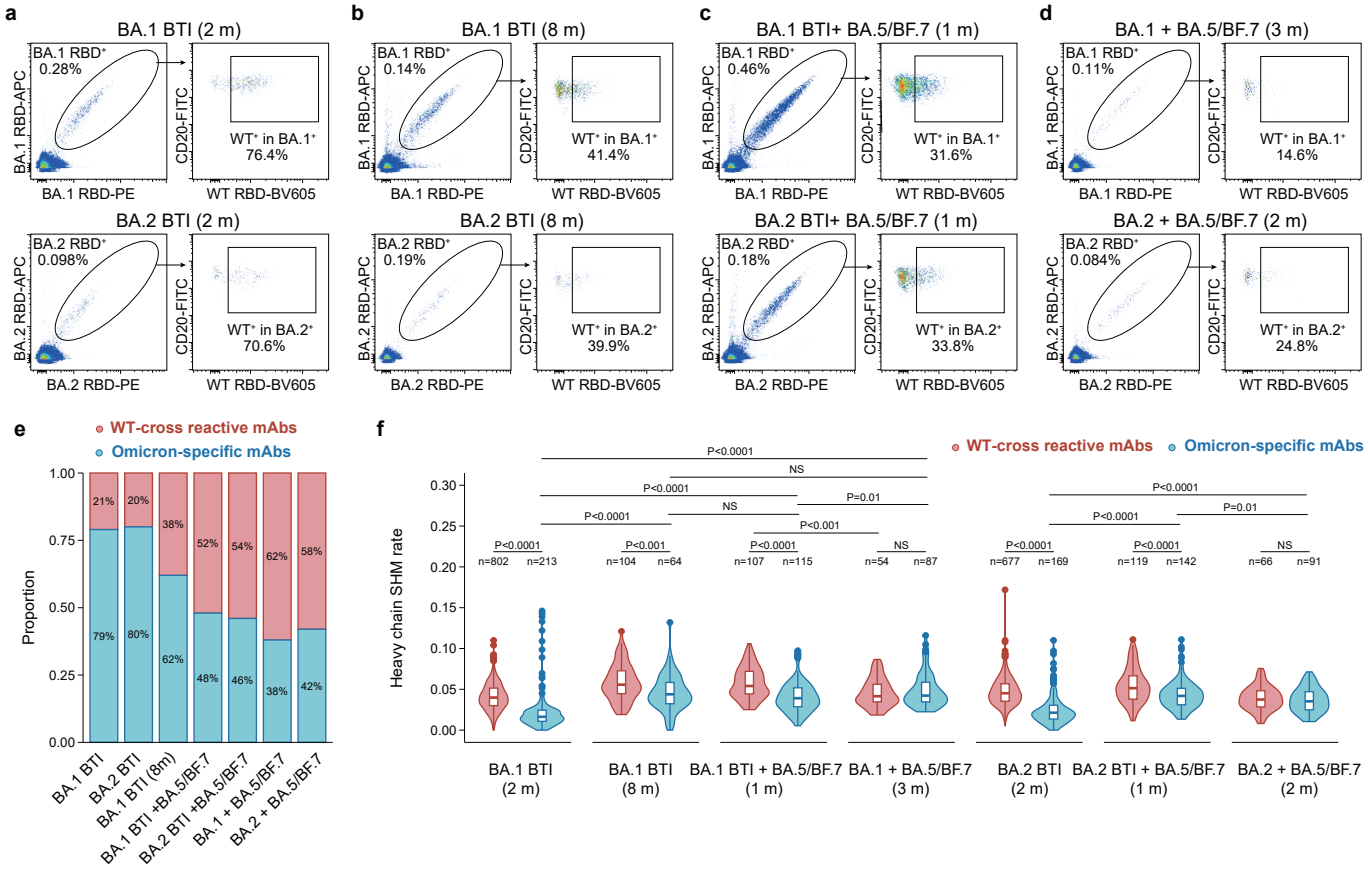

Fig.3 | B cell immune imprinting after repeated Omicron infections.
a–d, Flow cytometry analysis of pooled B cells from Omicron infection convalescent individuals. BA.1 (up) and BA.2 (down) RBD double-positive CD20+, IgM-, IgD-, CD27+ B cells were isolated for paired-single-cell V(D)J sequencing. Flow cytometry analyses were performed in cohorts of the following: (a) 2 months after BA.1 (up) or BA.2 (down) breakthrough infections, (b) 8 months after BA.1 (up) or BA.2 (down) breakthrough infections, (c) 1 month after BA.5/BF.7 reinfection after BA.1 (up) and BA.2 (down) breakthrough infections, (d) 2-3 months after BA.5/BF.7 reinfection after BA.1 (up) or BA.2 (down) infection without SARS-CoV-2 vaccination history. APC, allophycocyanine; FITC, fluorescein isothiocyanate; PE, phycoerythrin. BV605, Brilliant Violet 605. e, Proportions of WT-binding and non-WT-binding antibodies from Omicron breakthrough infection and repeated Omicron infection cohorts. Binding specificity was determined by ELISA. The antibodies were expressed in vitro using the sequence of the RBD-binding memory B cells from various cohorts. f, The heavy-chain variable domain somatic hypermutation (SHM) rate of the mAbs from various cohorts. Statistical tests were determined using two-tailed Wilcoxon rank-sum tests. Boxes display the 25th percentile, median and 75th percentile, and whiskers indicate median ± 1.5 times the interquartile range. Violin plots show kernel density estimation curves of the distribution. The numbers and ratios of samples in each group are labeled above the violin plots.

Figure 4

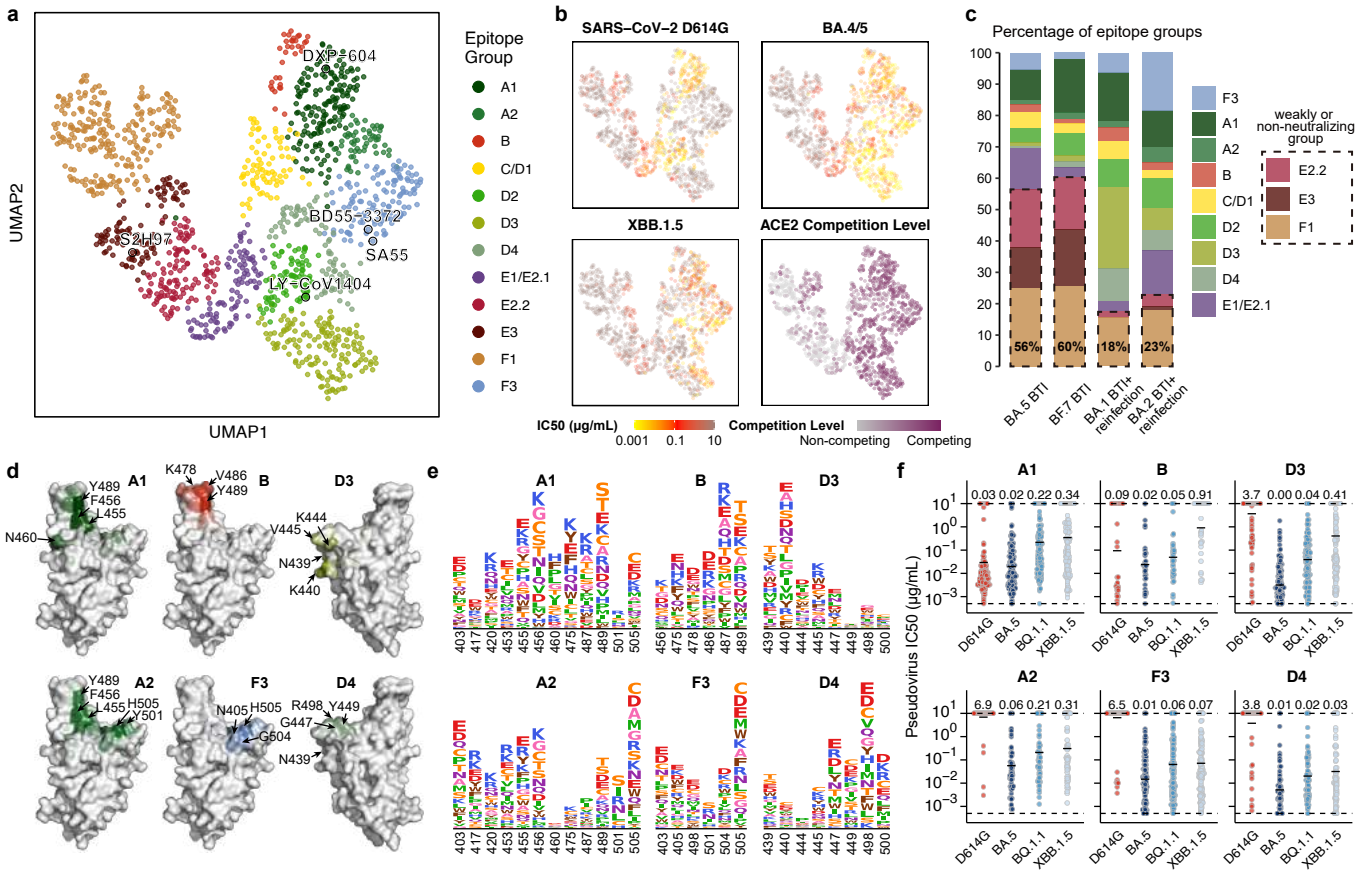

Fig. 4 | Epitope distribution and characterization of mAbs elicited by Omicron BTI and reinfection.
a, UMAP embedding of epitope groups of monoclonal antibodies (mAbs) binding BA.5 RBD isolated from convalescent individuals who experienced BA.5/BF.7 BTI or reinfection (n=1350). b, Neutralization activities, denoted as IC50 values, against SARS-CoV-2 D614G (n = 1349), BA.4/5 (n = 1322), and XBB.1.5 (n = 1346) spike-pseudotyped vesicular stomatitis viruses (VSV), as well as ACE2 competition levels determined by ELISA (n = 1344), are projected onto the UMAP embedding space. c, Distribution of mAbs across epitope groups is shown for BA.5 Breakthrough Infection (BTI), BF.7 BTI, BA.1 BTI with reinfection, and BA.2 BTI with reinfection. Epitope groups predominantly comprising non-neutralizing or weakly neutralizing mAbs (E2.2, E3, and F1) are highlighted with dashed boxes. The percentage of antibodies in these three groups is labeled on each bar. d, Average DMS escape scores of the crucial epitope groups contributing to neutralization against XBB.1.5 are illustrated on the structure model of the SARS-CoV-2 BA.5 RBD (PDB: 7XNS). Key residues with high escape scores for each group are labeled. e, The average DMS escape scores for the key epitope groups are represented as sequence logos; residues are depicted using the standard one-letter code and colored based on their chemical properties. The height of each letter corresponds to the escape score of the respective mutation. f, Pseudovirus-neutralization activities of mAbs within the six crucial epitope groups (A1 [n = 170], A2 [n = 60], B [n = 33], F3 [n = 129], D3 [n = 155], and D4 [n = 80]) are shown against SARS-CoV-2 D614G, BA.5, BQ.1.1, and XBB.1.5. Geometric mean IC50 values are displayed as bars and labeled above each group of data points.

Figure 5

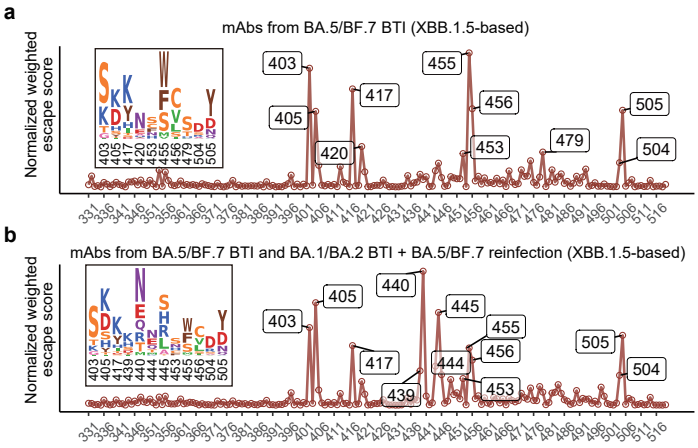

Fig. 5 | Estimate the evolutionary trends of XBB.1.5 RBD from DMS profiles.
Normalized average DMS escape scores weighted by IC50 against XBB.1.5 using DMS profiles of mAbs from BA.5/BF.7 BTI (a), and mAbs from BA.5/BF.7 BTI and BA.1/BA.2 BTI with BA.5/BF.7 reinfection (b). The impacts of each mutation on ACE2 binding and RBD expression, and the codon constraints on each residue, are also considered (see Methods). Residues with high estimated preferences are labeled, and their corresponding mutation scores are shown as logos.

Figure 6

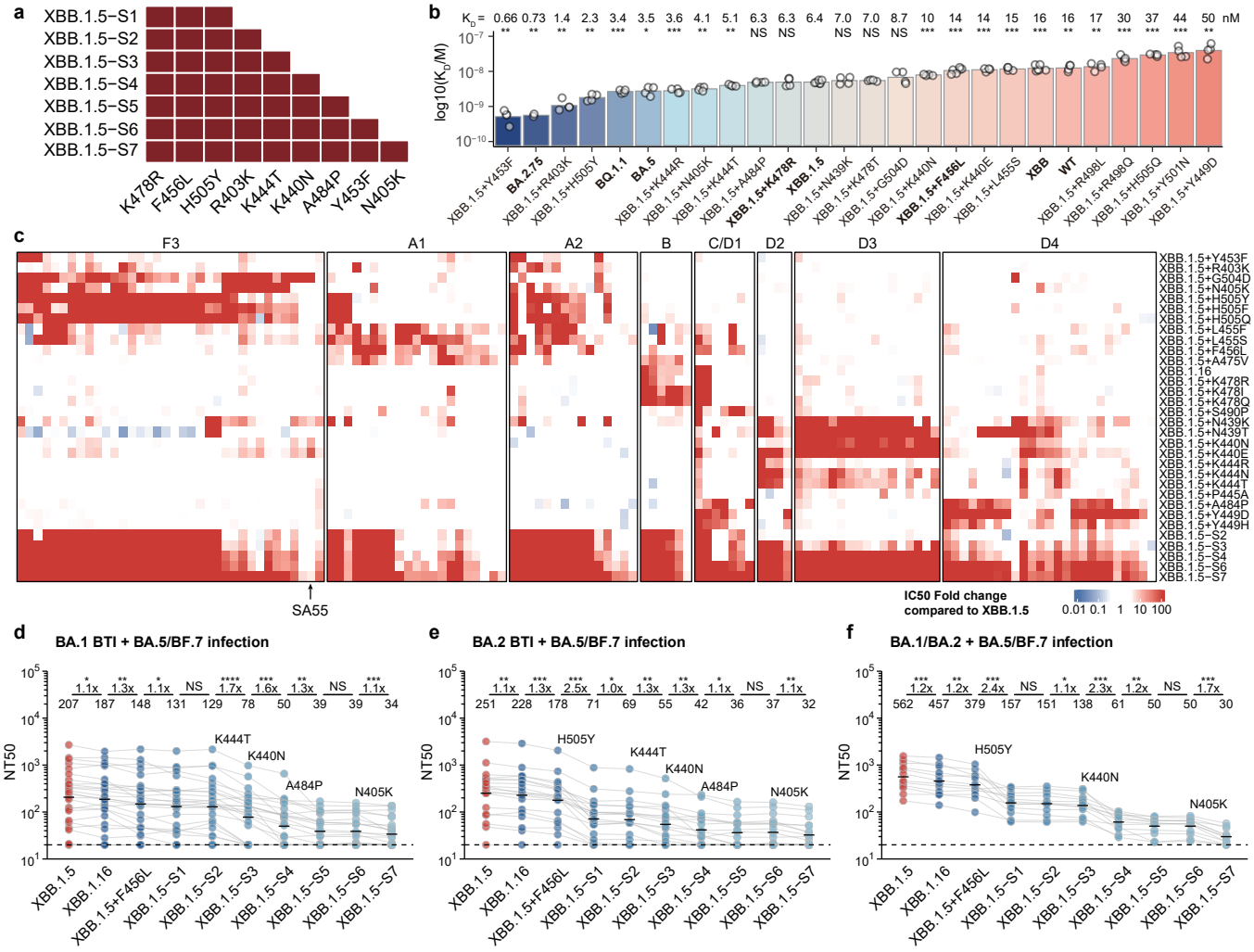

Fig. 6 | Combination of escape mutations evades XBB.1.5-neutralizing antibodies.
a, SARS-CoV-2 XBB.1.5-based pseudoviruses harboring combinations of critical mutations identified through analysis of DMS profiles are generated. b, hACE2-binding affinity for various RBD mutants of SARS-CoV-2 is assessed using SPR. Geometric mean dissociation constants (KD) from at least four independent replicates are shown, with statistical significance in comparison to XBB.1.5 RBD's KD labeled above the bars. P-values are determined using a two-tailed t-test on log-transformed KD values. c, IC50 values for representative potent XBB.1.5-neutralizing antibodies from different epitope groups against XBB.1.5 variants carrying individual or multiple escape mutations are displayed. Fold changes in IC50 against the mutants relative to XBB.1.5 are presented as a heatmap. d-f, Pseudovirus 50% neutralization titers (NT50) for SARS-CoV-2 XBB.1.5-based mutants are shown using plasma from convalescent individuals who experienced BA.5 or BF.7 reinfection: BA.1 BTI prior to BA.5/BF.7 reinfection (n = 26) (d); BA.2 BTI prior to BA.5/BF.7 reinfection (n = 19) (e); and reinfection with BA.5 or BF.7 after BA.1 or BA.2 infection without vaccination (n = 12) (f). Key mutations diminishing neutralization are labeled above their corresponding lines. Dashed lines indicate the limit of detection (LOD, NT50 = 20). Geometric mean titers are labeled above data points. Statistical tests are performed between neighboring mutants. P-values are calculated using two-tailed Wilcoxon signed-rank tests on paired samples. *p < 0.05, **p < 0.01, ***p<0.001, ****p<0.0001, and not significant (NS) p > 0.05.

Extended Data Figure 1

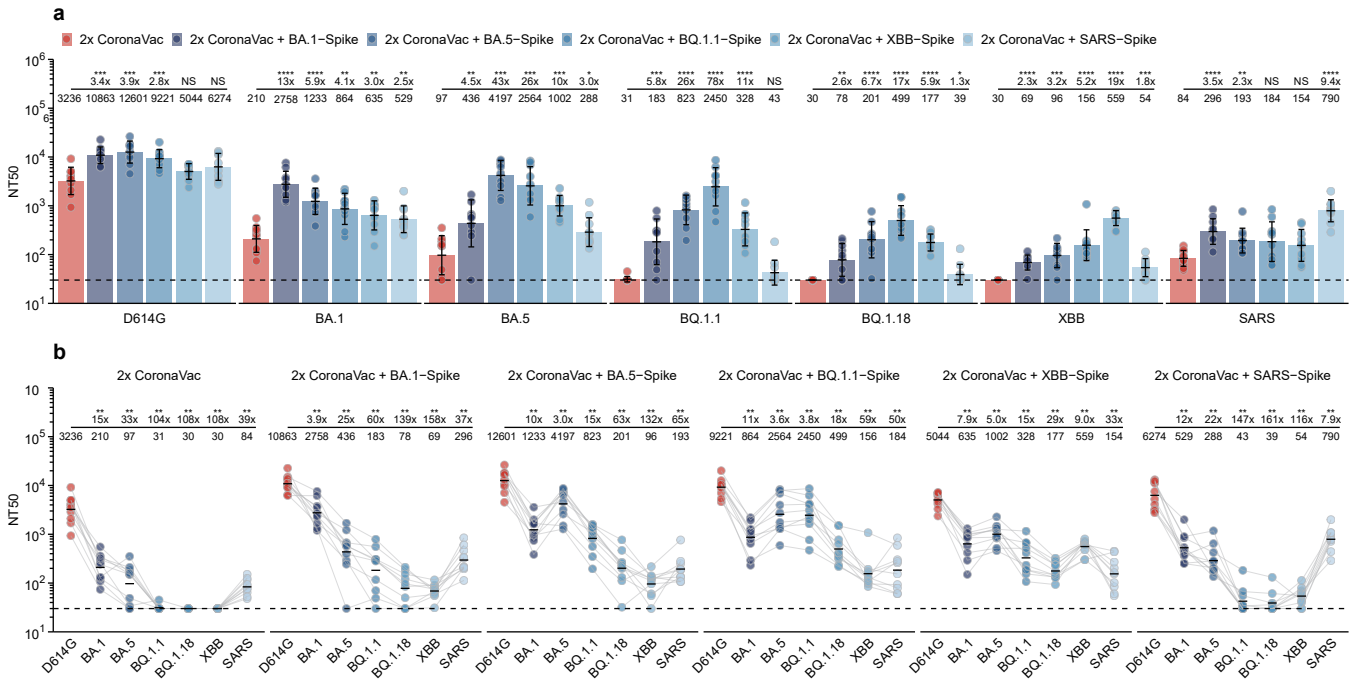

Extended Data Fig.1 | Neutralizing antibody response after CoronaVac primary and spike protein booster.
a, Comparison of neutralizing antibody responses among mouse immunization groups against pseudotyped D614G, SARS, and additional SARS-CoV-2 variants.. Mice sera antibody titers after priming with two doses of 3 μg CoronaVac followed by boosting with 10 μg SARS-CoV-1 Spike protein or SARS-CoV-2 variant Spike proteins in mice, or no boosting were measured. Fold changes between groups receiving different boosters and the primary-only group were calculated and shown above the line. Statistical significance was determined using the Wilcoxon rank sum test. b, Antibody breadth after priming with CoronaVac followed by boosting with different Spike proteins or no boosting. The neutralizing titer data used is the same as in a. Fold changes between titers against SARS or SARS-CoV-2 variants, and D614G were calculated and shown above the line. Statistical significance was determined using the Wilcoxon signed-rank test. *p < 0.05, **p < 0.01, ***p<0.001, ****p<0.0001, and not significant (NS) p > 0.05.

Extended Data Figure 2

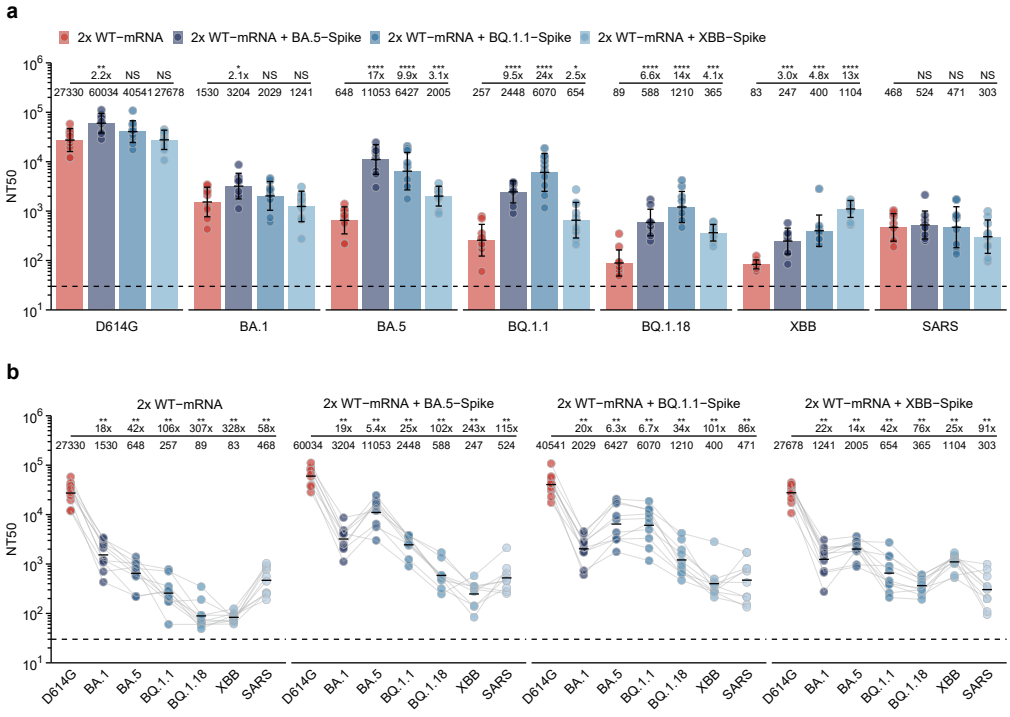

Extended Data Fig.2 | Neutralizing antibody response with mRNA vaccine as primary or booster.
a, Comparison of neutralizing antibody responses among mouse immunization groups against pseudotyped D614G, SARS, and additional SARS-CoV-2 variants. Mice sera antibody titers after priming with 2 doses of 10 μg WT-mRNA followed by boosting with 10 μg SARS-CoV-2 variant Spike proteins in mice, or no boosting were measured. Fold changes between groups receiving different boosters and the primary-only group were calculated and shown above the line. Statistical significance was determined using the Wilcoxon rank sum test. b, Antibody breadth after priming with WT-mRNA followed by boosting with SARS-CoV-2 variant Spike proteins in mice, or no boosting. The neutralizing titer data used is the same as in a. Fold changes between titers against SARS or SARS-CoV-2 variants, and D614G were calculated and shown above the line. Statistical significance was determined using the Wilcoxon signed-rank test. *p < 0.05, **p < 0.01, ***p<0.001, ****p<0.0001, and not significant (NS) p > 0.05.

Extended Data Figure 3

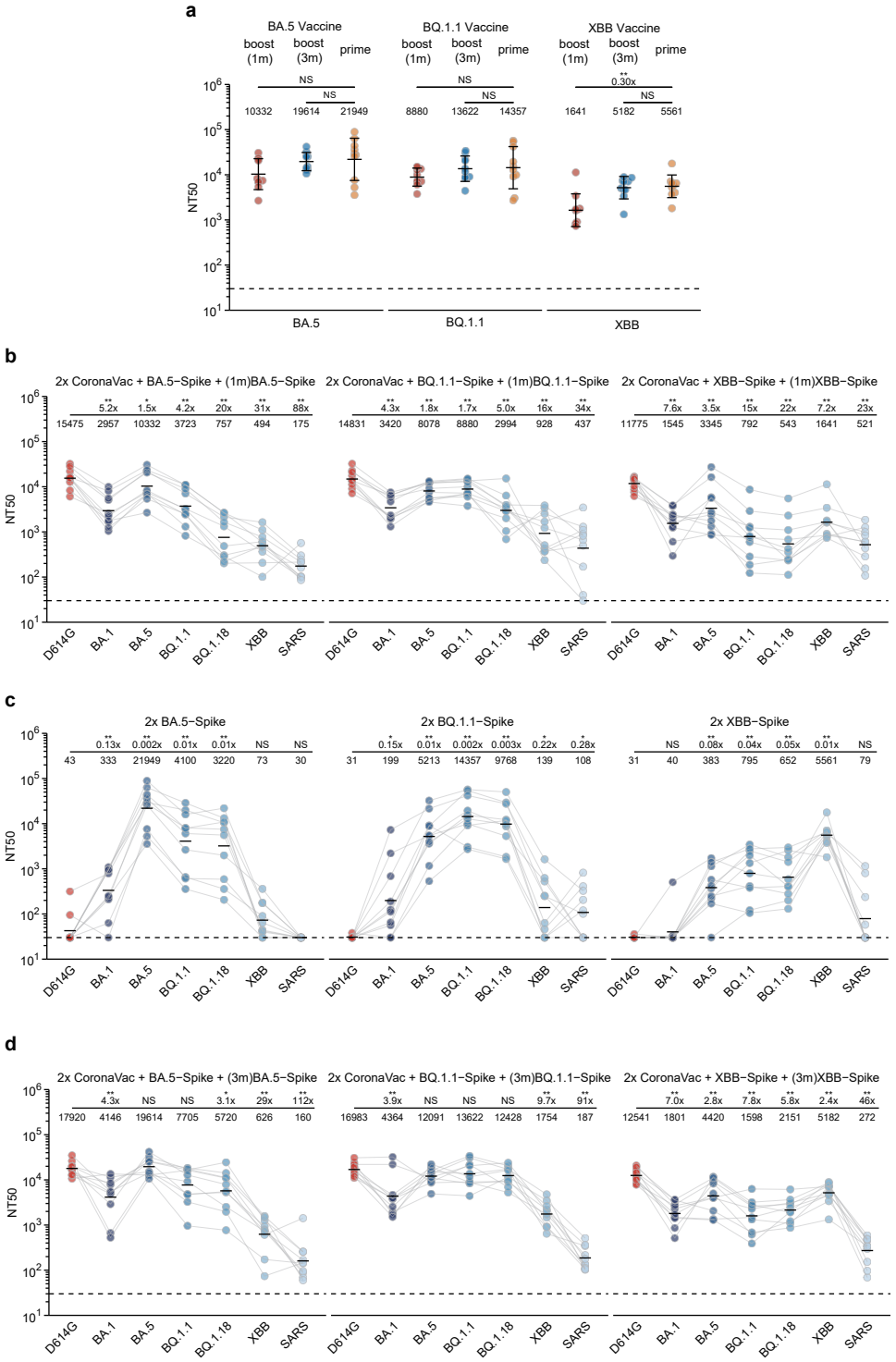

Extended Data Fig.3 | Comparison of neutralizing antibody responses with different intervals between the first and second Spike protein boosters.

a, Comparison of neutralizing antibody responses among different groups of mice immunized with 2 doses of CoronaVac, followed by two BA.5/BQ.1.1/XBB Spike protein boosters administered with one-month or three-month intervals between the first and second boosters, and compared to the primary immunization. Statistical significance was determined using the Wilcoxon rank sum test. b, Antibody breadth after priming with CoronaVac followed by boosting with 2 doses of BA.5/BQ.1.1/XBB Spike proteins with a one-month interval between the first and second boosters. Statistical significance was determined using the Wilcoxon signed-rank test. c, Antibody breadth after priming with 2 doses of BA.5/BQ.1.1/XBB Spike proteins. Statistical significance was determined using the Wilcoxon signed-rank test. d, Antibody breadth after priming with CoronaVac followed by boosting with 2 doses of BA.5/BQ.1.1/XBB Spike proteins with a three-month interval between the first and second boosters. Statistical significance was determined using the Wilcoxon signed-rank test. *p < 0.05, **p < 0.01, ***p<0.001, ****p<0.0001, and not significant (NS) p > 0.05.

Extended Data Figure 4

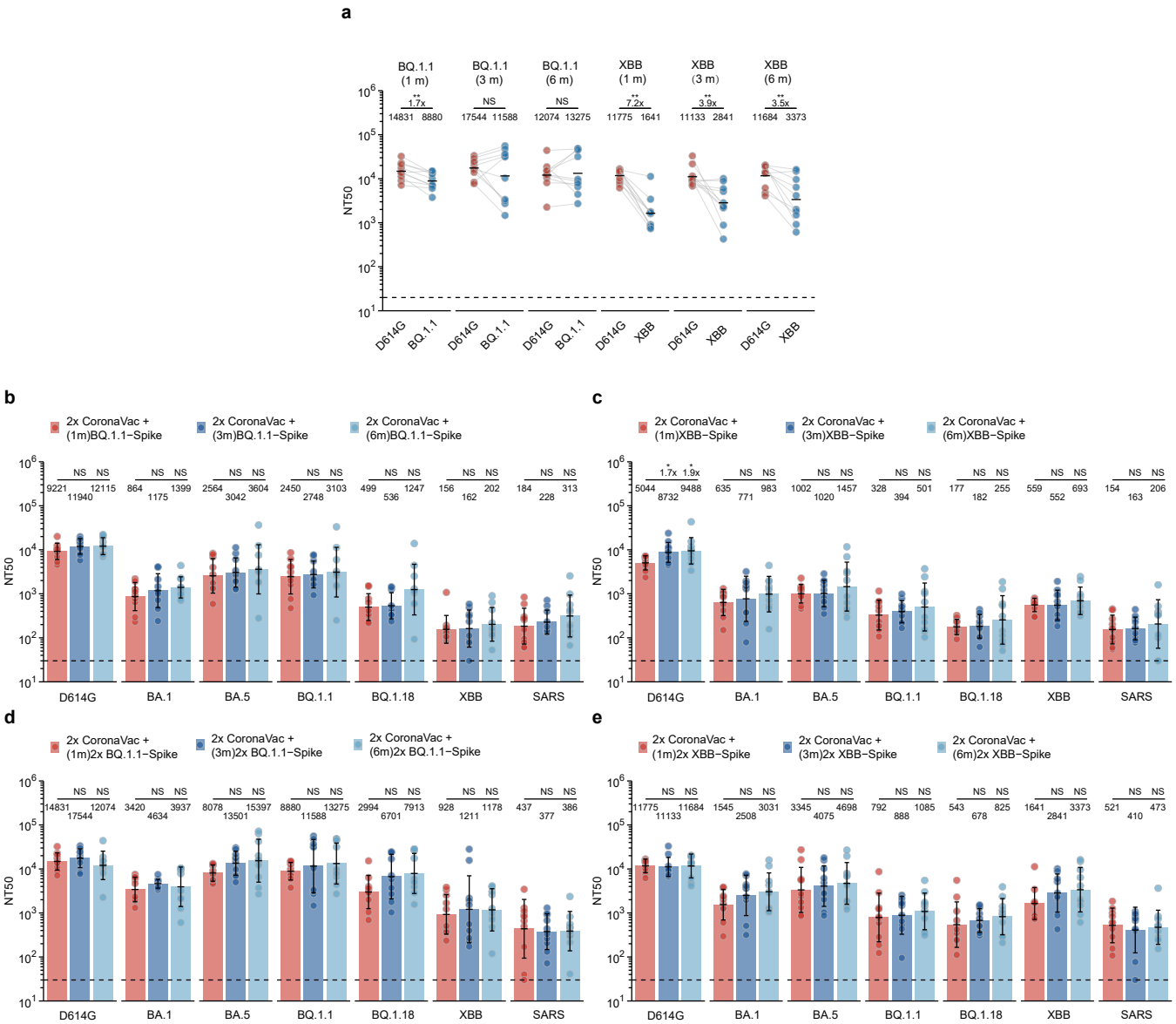

Extended Data Fig.4 | Comparison of neutralizing antibody responses with different intervals between primary vaccination and the first booster.

a, Comparison of neutralizing antibody responses among different groups of mice immunized with 2 doses of CoronaVac, followed by two additional doses of SARS-CoV-2 Spike protein vaccine at different intervals. Statistical significance was determined using the Wilcoxon signed-rank test. b-c, Comparison of neutralizing antibody responses among different groups of mice immunized with 2 doses of CoronaVac, followed by one dose of BQ.1.1(b) or XBB(c) Spike protein vaccine at different intervals. Statistical significance was determined using the Wilcoxon rank sum test. d-e, Comparison of neutralizing antibody responses among different groups of mice immunized with 2 doses of CoronaVac, followed by two additional doses of BQ.1.1(d) or XBB(e) Spike protein vaccine at different intervals. Statistical significance was determined using the Wilcoxon rank sum test. *p < 0.05, **p < 0.01, ***p<0.001, ****p<0.0001, and not significant (NS) p > 0.05.

Extended Data Figure 5

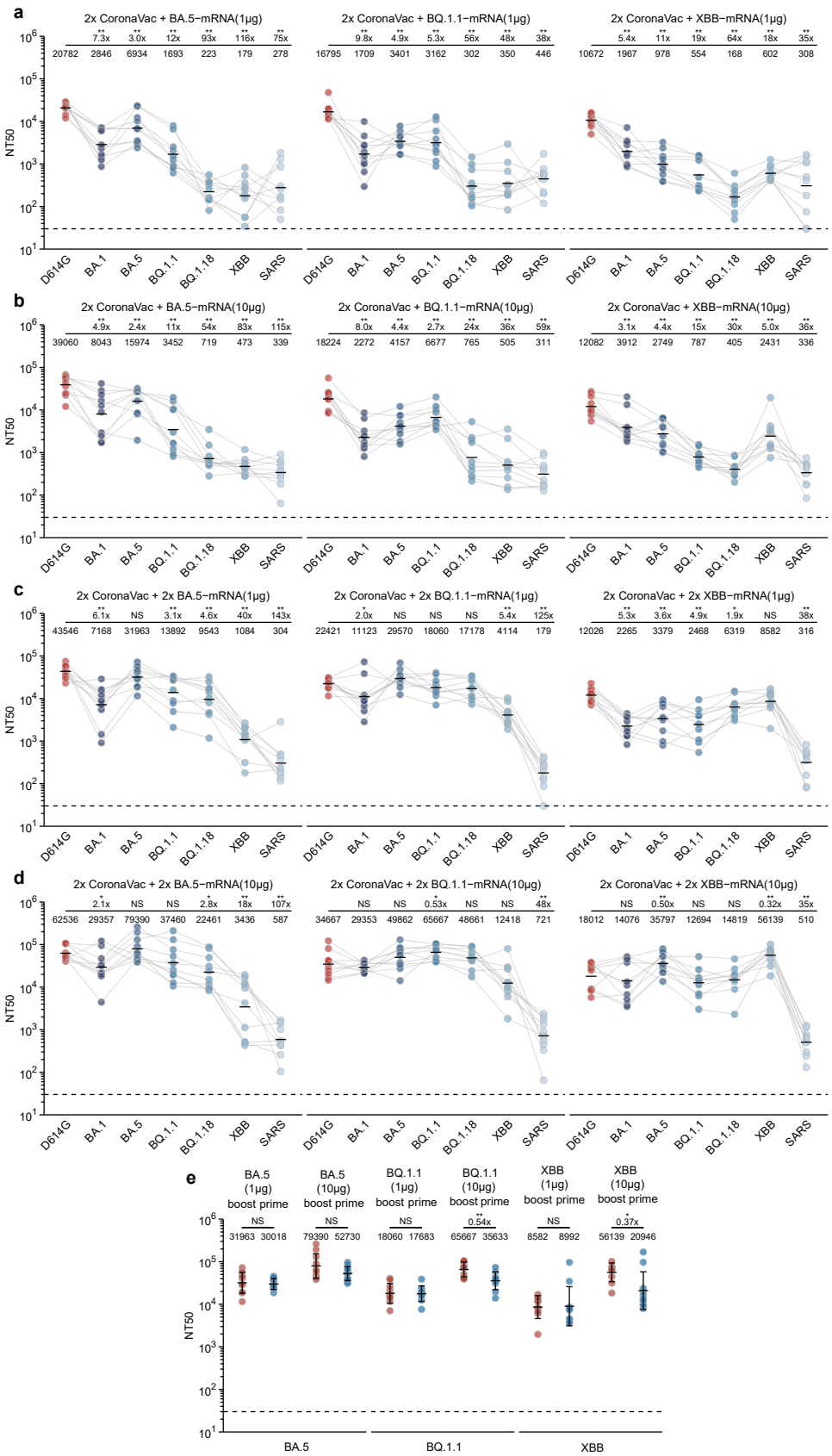

Extended Data Fig.5 | Comparison of neutralizing antibody responses with different mRNA vaccine booster dosages. a-b, Antibody breadth after priming with 2 doses of 3 μg CoronaVac followed by boosting with 1 dose of 1μg (a) or 10μg (b) BA.5/BQ.1.1/XBB Spike proteins in mice. Statistical significance was determined using the Wilcoxon signed-rank test. c-d, Antibody breadth after priming with 2 doses of 3 μg CoronaVac followed by boosting with 2 doses of 1μg (c) or 10μg (d) BA.5/BQ.1.1/XBB Spike proteins in mice. Statistical significance was determined using the Wilcoxon signed-rank test. e, Comparison of neutralizing antibody responses among different groups of mice immunized with 2 doses of CoronaVac, followed by 2 doses of BA.5/BQ.1.1/XBB mRNA boosters at different doses and compared to the primary immunization. Statistical significance was determined using the Wilcoxon rank sum test. *p < 0.05, **p < 0.01, ***p<0.001, ****p<0.0001, and not significant (NS) p > 0.05.

Extended Data Figure 6

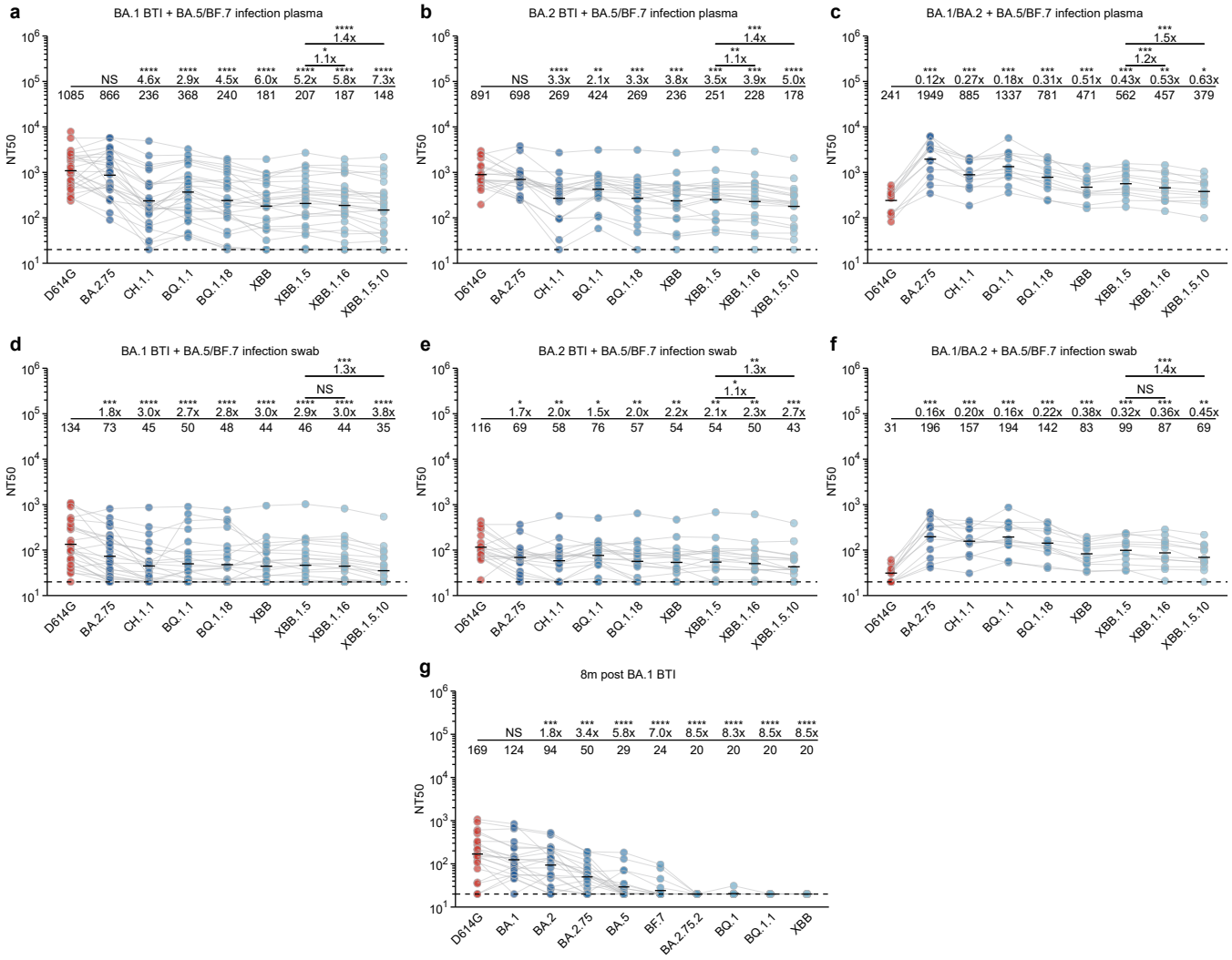

Extended Data Fig.6 | Antibody breadth of plasma and nasal swab after repeated Omicron infections.
a-c, Plasma antibody titers against pseudotyped D614G and variants after (a) BA.1 BTI + BA.5/BF.7 infection (n = 26), (b) BA.2 BTI + BA.5/BF.7 infection (n = 19), (c) BA.1/BA.2 + BA.5 infection (n = 12). d-f, Nasal swab antibody titers against pseudotyped D614G and variants after (d) BA.1 BTI + BA.5/BF.7 infection (n = 26), (e) BA.2 BTI + BA.5/BF.7 infection (n = 19), (f) BA.1/BA.2 + BA.5 infection (n = 12). g, Plasma antibody titers against pseudotyped D614G and variants after BA.1 BTI (n = 22). Fold changes between titers against variants and D614G were calculated and shown above the line in a-g. All statistical significance was determined using the Wilcoxon signed-rank test. *p < 0.05, **p < 0.01, ***p<0.001, ****p<0.0001, and not significant (NS) p > 0.05..

Extended Data Figure 7

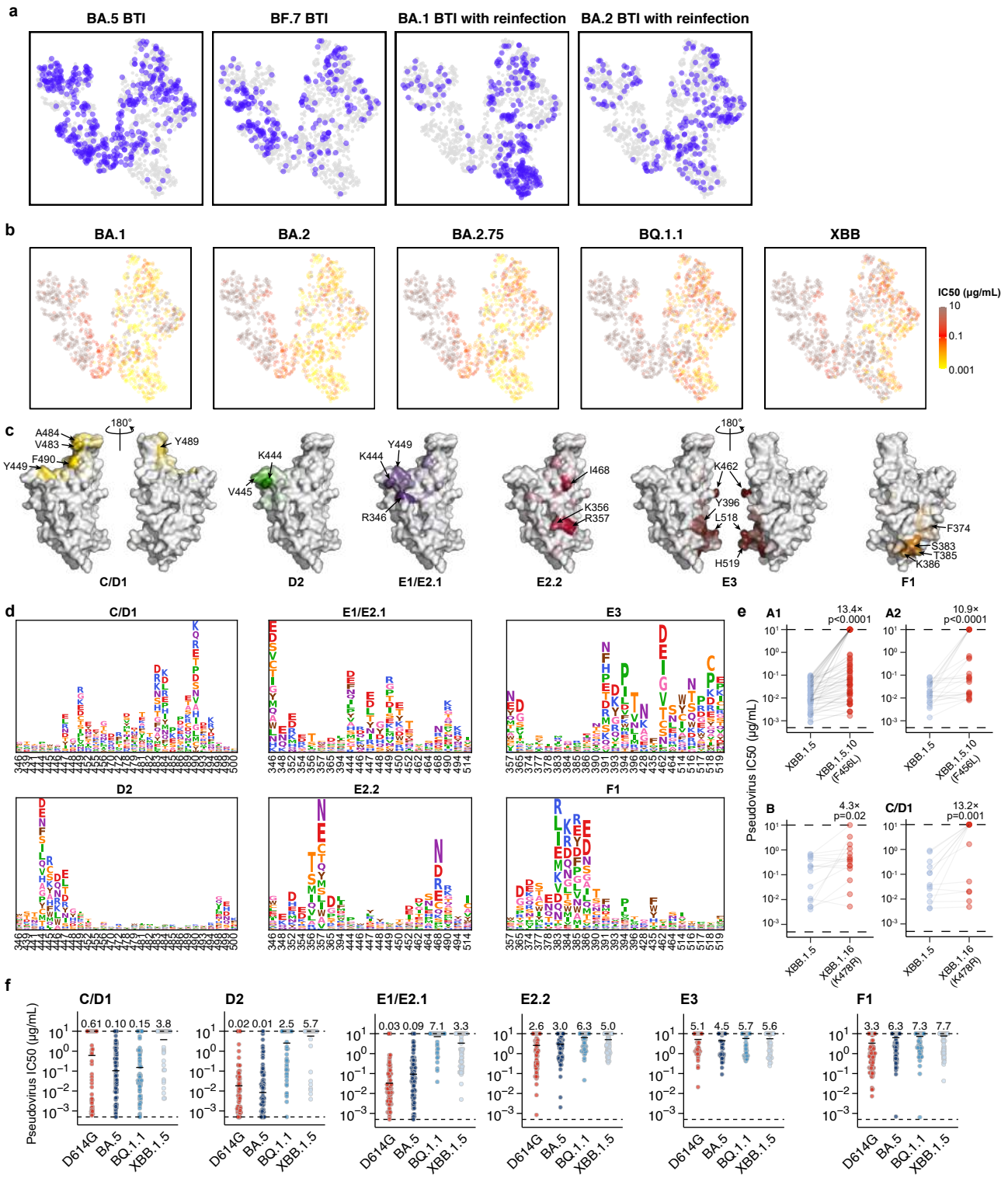

Extended Data Fig. 7 | Characteristics of BA.5-reactive mAbs elicited by BA.5/BF.7 BTI or reinfection.
a, Source of the antibodies are projected onto the UMAP embedding space. Antibodies from BA.5 BTI (n=445), BF.7 BTI (n=243), BA.1 BTI with reinfection (n=284), and BA.2 BTI with reinfection (n=232) are colored blue in the corresponding panel, and other antibodies are gray. b, Neutralization activities, denoted as IC50 values, against SARS-CoV-2 BA.1 (n = 1260), BA.2 (n = 1238), BA.2.75 (n=1238), BQ.1.1 (n = 1335) and XBB (n = 1341) spike-pseudotyped VSV are projected onto the UMAP embedding space. c, Average escape scores of epitope groups that are not shown in Fig. 4d (C/D1, D2, E1/E2.1, E2.2, E3, and F1) are illustrated on the structure model of the SARS-CoV-2 BA.5 RBD (PDB: 7XNS). Key residues with high escape scores for each group are labeled. d, Average DMS escape scores for these epitope groups are represented as sequence logos; residues are depicted using the standard one-letter code and colored based on their chemical properties. The height of each letter corresponds to the escape score of the respective mutation. e, Pseudovirus-neutralization activities of XBB.1.5-neutralizing mAbs in groups A1 (n=70) and A2 (n=23) against XBB.1.5 and XBB.1.5.10; and mAbs in groups B (n=15) and C/D1 (n=13) against XBB.1.5 and XBB.1.16. Fold changes in IC50 are labeled. P-values are calculated using two-tailed Wilcoxon signed-rank test of paired samples. f, Pseudovirus-neutralization activities of mAbs within the six crucial epitope groups (C/D1 [n = 76], D2 [n = 86], E1/E2.1 [n = 100], E2.2 [n = 124], E3 [n = 101], and F1 [n = 236]) are shown against SARS-CoV-2 D614G, BA.5, BQ.1.1, and XBB.1.5. Geometric mean IC50 values are displayed as bars and labeled above each group of data points.

Extended Data Figure 8

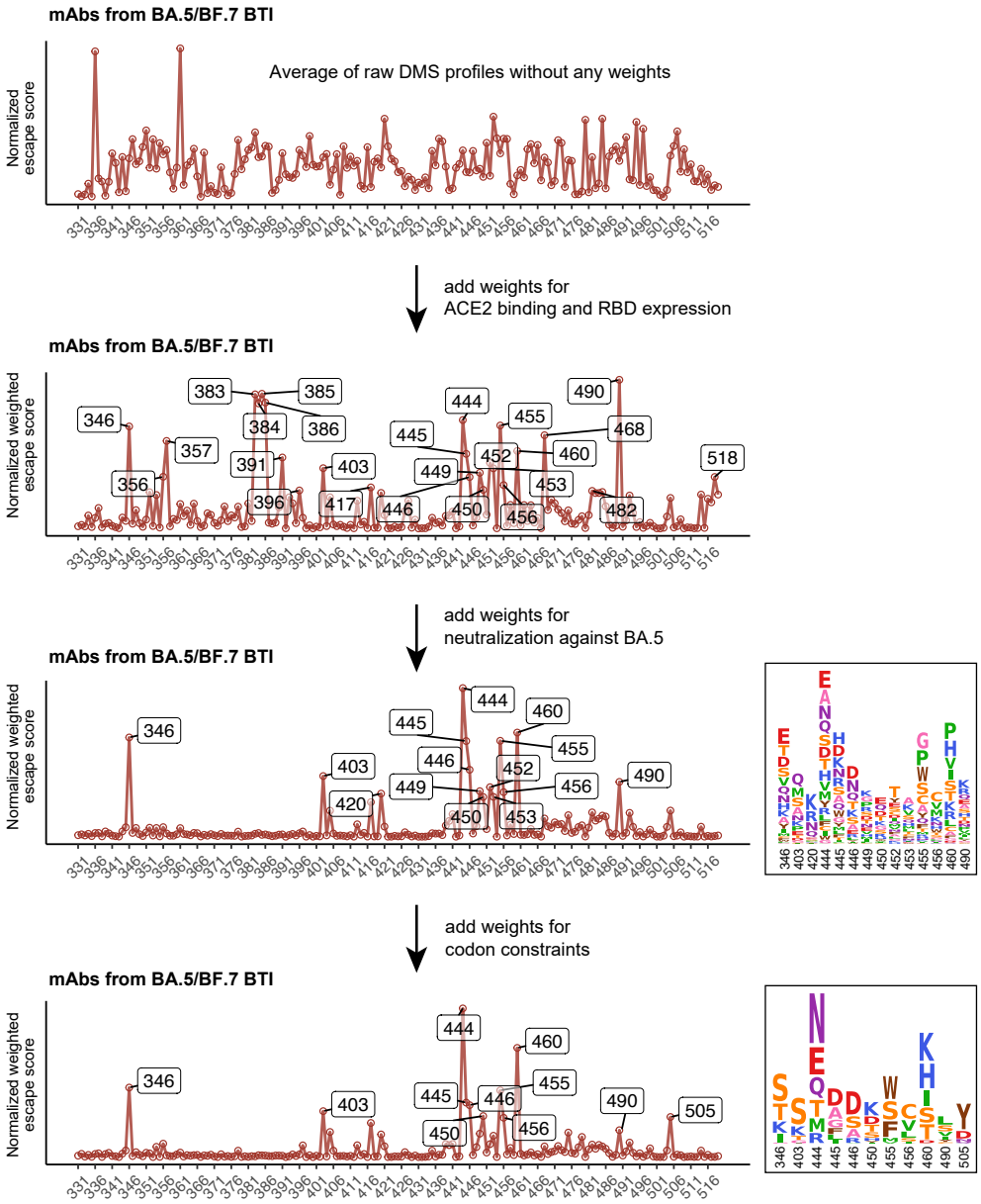

Extended Data Fig. 8 | Workflow of calculating weighted escape scores of each mutation on RBD. Weights for ACE2 binding and RBD expression, neutralization activity, and codon usage are sequentially applied on the calculation to achieve informative results. Mutation preferences of BA.5 RBD under the pressure of NAbs from BA.5 or BF.7 BTI are shown.

Extended Data Figure 9

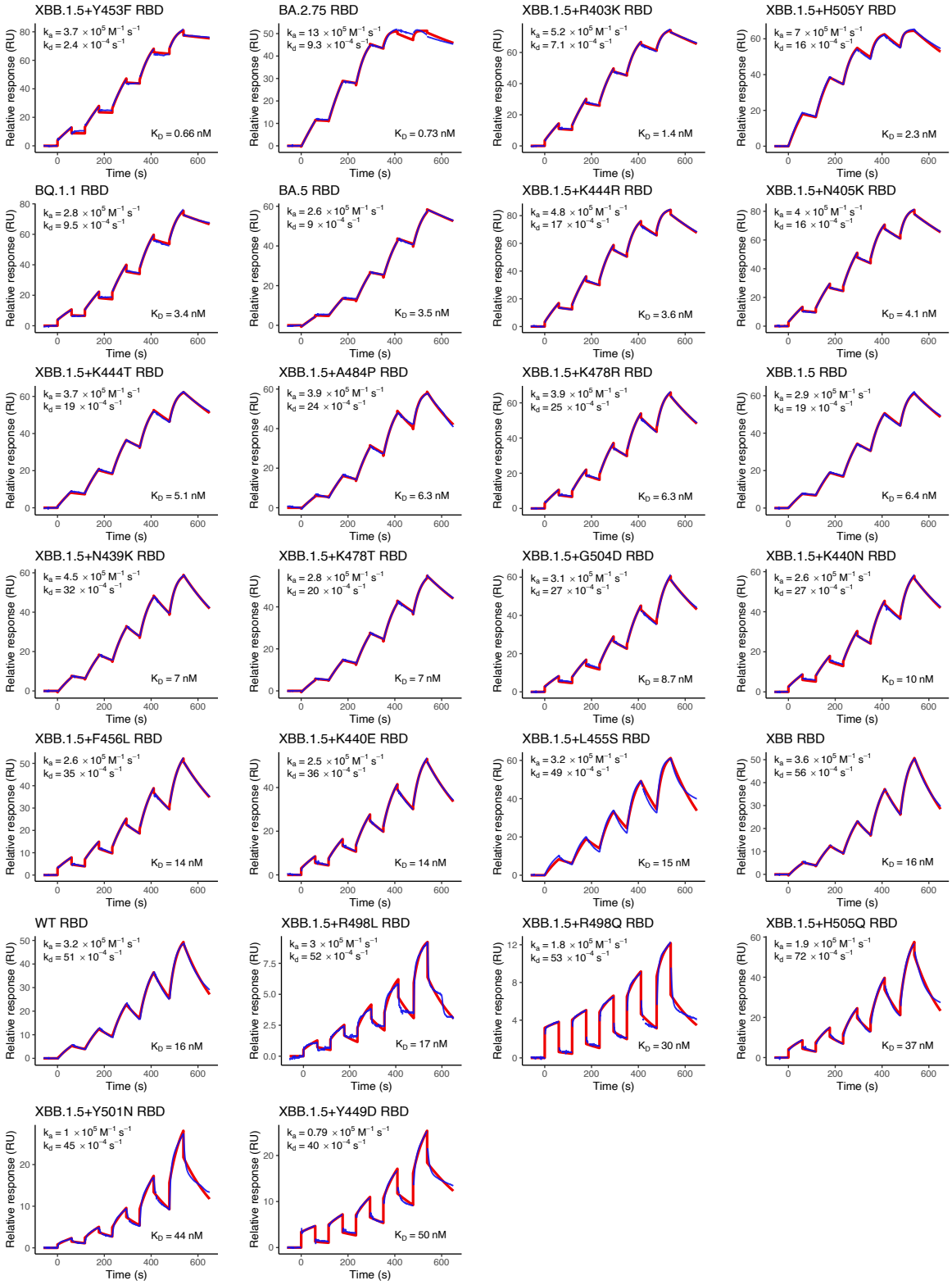

Extended Data Fig. 9 | SPR sensorgrams for affinity of hACE2 and SARS-CoV-2 mutants RBD
Representative sensorgram of at least four replicates is shown for each RBD. Geometric mean kinetic constants k_a, k_d, and dissociation equilibrium constant (K_D) are labeled in each panel.

Extended Data Figure 10

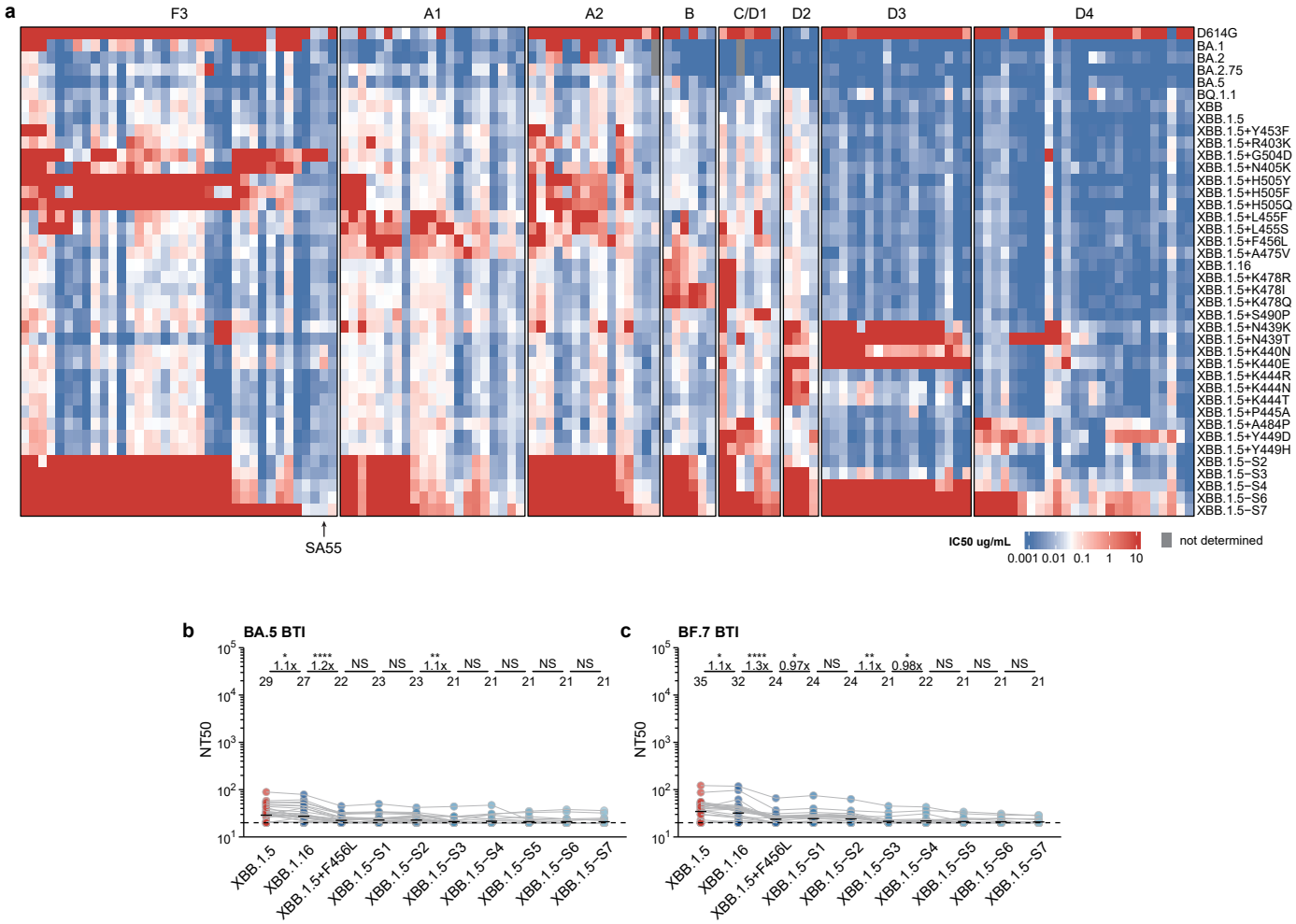

Extended Data Fig. 10 | NAbs from BTI and reinfection are escaped by constructed mutants.
a, IC50 values for representative potent XBB.1.5-neutralizing antibodies from different epitope groups against XBB.1.5 variants carrying individual or multiple escape mutations are shown. The order of antibodies is the same as that in Fig. 6c. b, Pseudovirus NT50 for SARS-CoV-2 XBB.1.5-based mutants are shown using plasma from convalescent individuals who experienced BA.5 (n=36) or BF.7 BTI (n = 30). Statistical tests are performed between neighboring mutants. P-values are calculated using two-tailed Wilcoxon signed-rank tests on paired samples. *p < 0.05, **p < 0.01, ****p < 0.0001, and p > 0.05 (NS).